Redox Biology 59 (2023) 102589

Contents lists available at ScienceDirect

Redox Biology

journal homepage: www.elsevier.com/locate/redox

Enhancement of glycolysis-dependent DNA repair regulated by *FOXO1* knockdown via PFKFB3 attenuates hyperglycemia-induced endothelial oxidative stress injury

Dandan Sun [a,b,1], Shimei Chen [a,b,1], Shenping Li [a,b], Ning Wang [a,b], Shuchang Zhang [a,b], Li Xu [a,b], Shaopin Zhu [a,b], Huiming Li [a], Qing Gu [a,b], Xun Xu [a,b,**], Fang Wei [a,b,*]

[a] *Department of Ophthalmology, Shanghai General Hospital, Shanghai Jiao Tong University School of Medicine, Shanghai, 200080, China*
[b] *National Clinical Research Center for Eye Diseases, Shanghai Key Laboratory of Ocular Fundus Disease, Shanghai Engineering Center for Visual Science and Photo Medicine, Shanghai Engineering Center for Precise Diagnosis and Treatment of Eye Diseases, Shanghai, 200080, China*

ARTICLE INFO

Keywords:
Diabetes
Endothelial cell
Oxidative stress
DNA damage
DNA repair
Glycolysis

ABSTRACT

The accumulation of DNA damage induced by oxidative stress is a crucial pathogenic factor of endothelial loss in diabetic vascular complications, but it is still unknown whether aberrant glucose metabolism leads to defective DNA repair and accounts for hyperglycemia-induced endothelial oxidative stress injury. Here, we showed that *Foxo1* knockdown alleviated diabetes-associated retinal DNA damage and vascular dysfunction. Mechanistically, *FOXO1* knockdown avoided persistent DNA damage and cellular senescence under high glucose in endothelial cells by promoting DNA repair mediated by the MRN (MRE11-RAD50-NBS1 complex)-ATM pathway in response to oxidative stress injury. Moreover, *FOXO1* knockdown mediated robust DNA repair by restoring glycolysis capacity under high glucose. During this process, the key glycolytic enzyme PFKFB3 was stimulated and, in addition to its promoting effect on glycolysis, directly participated in DNA repair. Under genotoxic stress, PFKFB3 relocated into oxidative stress-induced DNA damage sites and promoted DNA repair by interaction with the MRN-ATM pathway. Our study proposed that defective glycolysis-dependent DNA repair is present in diabetic endothelial cells and contributes to hyperglycemia-induced vascular dysfunction, which could provide novel therapeutic targets for diabetic vascular complications.

1. Introduction

Diabetic cardiovascular disease and microvascular complications, such as diabetic retinopathy (DR), are the leading cause of morbidity and mortality in people with diabetes [1] and the prevalence of diabetic vascular complications has been increasing rapidly [2]. A key event of diabetic vascular complications is increased vascular permeability with the loss of endothelial cells (ECs) [3].

The unifying mechanism [4,5] has drawn attention to the role of oxidative stress-induced DNA damage in the pathologies of diabetic ECs: Increased reactive oxygen species (ROS) cause DNA damage and overactivation of DNA repair enzyme poly (ADP-ribose) polymerase (PARP), which modifies glyceraldehyde-3 phosphate dehydrogenase (GAPDH) with poly-ADP-ribose by consuming the intracellular nicotinamide adenine dinucleotide (NAD) pool and impairs glycolysis. Glucose is, therefore, fluxed into side branching pathways, including the polyol pathway, formation of intracellular advanced glycation end products (AGEs), protein kinase C (PKC) pathway, and hexosamine pathway. Although previous studies have confirmed that the increasing DNA damage accounts for diabetic vasculopathy [6–9]、diabetes-related pulmonary and renal fibrosis [10], it is currently unclear whether defective DNA repair leads to DNA damage together with oxidative stress during the loss of diabetic ECs. To date, studies on impaired DNA repair in diabetes feature extensive analyses of DNA damage markers and the genetic polymorphisms and gene expression of DNA damage repair enzymes [11–14] but lack research on specific mechanisms. Our previous study [15] has revealed that defective DNA repair leads to the accumulation of DNA damage together with oxidative stress during the loss of diabetic ECs. Here, we further explored the molecular

* Corresponding author. No. 100 Haining Road, Hongkou District, Shanghai, 200080, China.
** Corresponding author. No. 100 Haining Road, Hongkou District, Shanghai, 200080, China.
E-mail addresses: drxuxun@sjtu.edu.cn (X. Xu), weifang73@hotmail.com (F. Wei).
[1] These two authors are co-first authors and contributed equally to the study.

https://doi.org/10.1016/j.redox.2022.102589
Received 3 November 2022; Received in revised form 14 December 2022; Accepted 23 December 2022
Available online 25 December 2022

Abbreviations

Ad	adenovirus
AGE	advanced glycation end product
ATM	ataxia telangiectasia mutated
ATR	ATM and RAD3-related
DNA-PK	DNA-dependent protein kinase
DR	diabetic retinopathy
DRR	DNA repair reporter
DSB	DNA double-strand break
DSBR	DSB repair
EB	Evans blue
EC	endothelial cell
ECAR	extracellular acidification rate
GAPDH	glyceraldehyde-3 phosphate dehydrogenase
HR	homologous recombination repair
HUVEC	human umbilical vein endothelial cell
MRN	MRE11-RAD50-NBS1 complex
NAD	Nicotinamide adenine dinucleotide
NHEJ	non-homologous end joining
OCR	oxygen consumption rate
OLIGO	oligomycin
PARP	poly (ADP-ribose) polymerase
PFA	paraformaldehyde
PFK	phosphofructokinase
PFKFB3	phosphofructo-2-kinase/fructose-2,6-bisphosphatase 3
PKC	protein kinase C
PKM	pyruvate kinase
qPCR	quantitative real-time PCR
ROS	reactive oxygen species
ROT/AA	rotenone/antimycin
SA-β-Gal	senescence-associated-β-galactosidase
SD	standard deviation
γH2AX	phosphorylated H2AX
2DG	2-deoxy-glucose

mechanisms of DNA repair impairment from the metabolic perspective as diabetes is a metabolic disease.

The Forkhead box transcription factor O1 (FOXO1) has multiple roles in diabetic pathology [16–20]. The regulation of systemic glucose metabolism by FOXO1 in hepatocytes has been extensively studied [21–23] while Wilhelm et al. have reported that FOXO1 also serves as an essential regulator of vascular growth, which couples metabolic and proliferative activities in ECs by reducing a series of associated gene expression with glycolysis and mitochondrial respiration [24]. FOXO1 has been reported to participate in the endothelial loss in DR by increasing apoptosis [25]. However, whether the metabolic abnormality induced by FOXO1 plays a part in the loss of diabetic ECs or affects DNA repair function remains unknown since metabolic homeostasis is crucial for ECs to coordinate responses to environmental stress [26].

In the present study, we revealed for the first time how aberrant glucose metabolism impairs DNA repair in response to oxidative stress injury in ECs. Through the knockdown of *FOXO1*, we provided conclusive evidence that maladaptive glycolysis hindered DNA repair and led to persistent oxidative stress injury in ECs under high glucose and retinal vascular dysfunction in diabetic mice, which were rescued by *FOXO1* knockdown. We also revealed that 6-phosphofructo-2-kinase/fructose-2,6-bisphosphatase 3 (PFKFB3), a key glycolytic enzyme stimulated by *FOXO1* knockdown, directly participated in DNA repair, in addition to its promoting effect on glycolysis in ECs. We demonstrated that PFKFB3 relocated into oxidative stress-induced DNA damage sites and facilitated DNA repair by interaction with the MRN (MRE11-RAD50-NBS1 complex)-ATM pathway in ECs. This study characterized impaired glycolysis-dependent DNA repair in response to oxidative stress injury in diabetic ECs, which may be a target for vascular protection in diabetes.

2. Results

2.1. Foxo1 knockdown attenuates oxidative stress damage in diabetic mouse retina

Consistent with a previous study [25], the FOXO1 protein level increased and was mainly concentrated in the nuclei of ECs in the retinal vascular net of diabetic mice (Fig. 1A–C). DNA double-strand breaks (DSBs) are the most toxic among various forms of DNA damage, threatening chromosomal stability and cell survival if not repaired correctly. Thus, we detected phosphorylated H2AX (γH2AX) foci, a sensitive marker of DSBs, in immunofluorescence staining and determined the protein level of γH2AX and PARP1 to confirm if the accumulation of oxidative DNA damage existed in the retinas of diabetic mice. The level of γH2AX and PARP1 increased significantly in the retinas of diabetic mice, while adenoviruses for *Foxo1* knockdown decreased the protein level of γH2AX and PARP1 and the accumulation of γH2AX foci (Fig. 1B–D), demonstrating its potential protective effect against diabetes-induced DNA damage.

Next, Evans blue (EB) assays were conducted to detect retinal vascular leakage, and retinal trypsin digestion assays were conducted to measure the number of acellular capillaries. *Foxo1* knockdown significantly reduced retinal vascular leakage and acellular capillary number induced by high glucose (Fig. 1E–H). TUNEL assay was conducted to determine the apoptosis of the whole retinas, showing that *Foxo1* knockdown reduced excessive apoptosis in the diabetic retinas (Fig. S1A).

2.2. FOXO1 knockdown reduces oxidative stress-induced DNA damage and cellular senescence in HUVECs under high glucose

Similarly, high glucose increased both the FOXO1 protein levels in the whole cell and in the nucleus of human umbilical vein endothelial cells (HUVECs) (Fig. 2A and B). To further confirm the effect of *FOXO1* knockdown on the improvement of oxidative stress-induced DNA damage under high glucose in vitro, we treated HUVECs with H_2O_2, one major form of reactive oxygen species, to induce moderate DNA damage. Immunofluorescence microscopy was conducted to illustrate further the distribution of FOXO1. FOXO1 was distributed more evenly in the nuclei and plasma in the control group, while high glucose increased its concentration in the nuclei with and without H_2O_2 treatment (Fig. 2C).

The γH2AX level was measured and the comet assay was conducted to determine the DNA damage level. Notably, the increased γH2AX under high glucose was reversed by the *FOXO1* knockdown with and without H_2O_2 (Fig. 2D–F). DNA damage caused by high glucose alone was not detectable using comet assay (Fig. S1B), as more than 20% DNA in the tail is recommended in the comet assay considering the recovery capacity of cells [27]. After H_2O_2 treatment, the average tail moment under high glucose, which was higher than that of the control group, declined after *FOXO1* knockdown (Fig. 2G and H), indicating that the recovery from H_2O_2-induced DNA damage was severely impaired after high glucose treatment, but it was rescued by *FOXO1* knockdown. As persistent nuclear DNA damage is causatively associated with cellular senescence [28], SA-β-Gal activity was conducted to determine the degree of cellular senescence. It showed that *FOXO1* knockdown alleviated aggravated cellular senescence under high glucose with and without H_2O_2 treatment (Fig. 2I and J, and Figs. S1C and D).

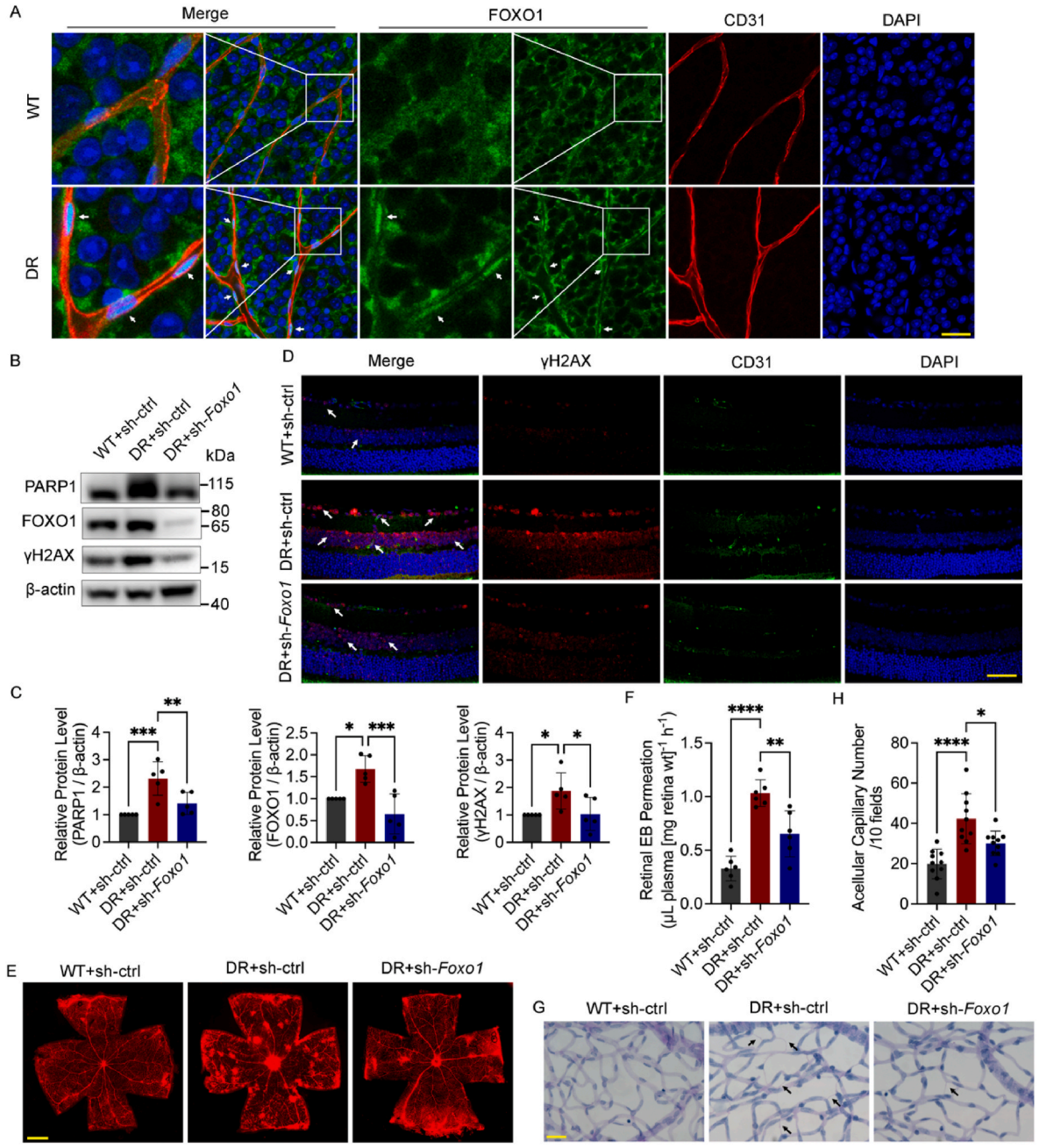

Fig. 1. *Foxo1* knockdown attenuates oxidative stress damage in diabetic mouse retina. **A** The localization of FOXO1 in the retina of nondiabetic C57BL/6 mice (WT) and diabetic mice (DR). White arrows indicate the nuclear translocation of FOXO1. n = 12. Scale bar, 100 μm. **B** and **C** Western blot analysis of PARP1, FOXO1 and γH2AX in the whole retina extracts. WT and DR mice received the intravitreal injection of adenovirus (Ads) for *Foxo1* knockdown (sh-*Foxo1*), or vehicle controls (sh-ctrl) as indicated. n = 10. **D** Immunofluorescence staining of γH2AX. White arrows indicate γH2AX foci. n = 12. Scale bar, 50 μm. **E** and **F** Retinal vascular leakage assessed by Evans blue (EB) dye. The confocal analysis of whole-mounted retinas (**E**, scale bar: 500 μm) and statistical results of spectrophotometrically measured EB extravasation (**F**) are shown. n = 12. **G** and **H** The number of acellular capillaries. Scale bar, 20 μm. n = 10. Black arrows indicate acellular capillaries. All results are displayed as means ± SD. $^{*}P < 0.05$, $^{**}P < 0.01$, $^{***}P < 0.001$, $^{****}P < 0.0001$, one-way ANOVA analysis. (For interpretation of the references to color in this figure legend, the reader is referred to the Web version of this article.)

2.3. *FOXO1* knockdown alleviates oxidative stress-induced DNA damage by enhancing DNA repair mediated by the MRN-ATM pathway

To gain an insight into the role of *FOXO1* knockdown behind its enhancement of the recovery from oxidative stress-induced DNA damage, the intracellular ROS level was measured to determine if the source of DNA damage was reduced. However, *FOXO1* knockdown did not reduce the intracellular ROS in the high glucose group (Fig. S2A), indicating that *FOXO1* knockdown alleviated DNA damage independent of direct anti-oxidative mechanism. Thus, we next evaluated the level of DNA repair function employing the DNA repair reporter (DRR) assay. The activity of two major DSB repair (DSBR) pathways, homologous recombination (HR) and non-homologous end joining (NHEJ) repair, decreased in high glucose but was ameliorated by *FOXO1* knockdown (Fig. 3A and B).

Ataxia telangiectasia mutated (ATM), ATM and RAD3-related (ATR), and the DNA-dependent protein kinase (DNA-PK) are three critical PI3Ks in the DNA damage responses, which are indispensable for initiating the subsequent DSBR [29]. As *FOXO1* knockdown improved DSBR activity, we next investigated if this effect would collapse upon the

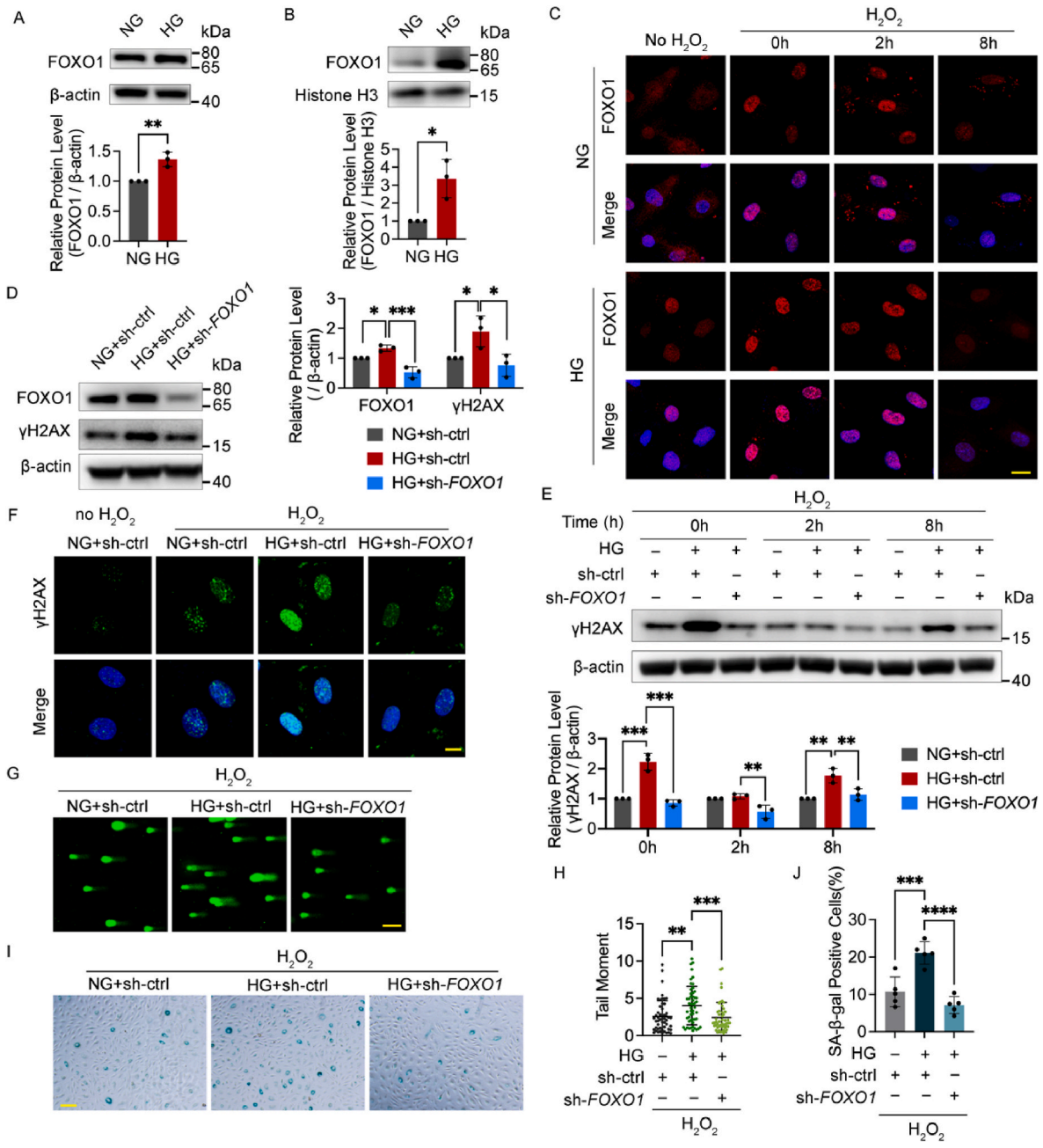

Fig. 2. *FOXO1* knockdown reduces oxidative stress-induced DNA damage and cellular senescence in HUVECs under high glucose. **A** and **B** Western blot analysis of FOXO1 in the whole cell extracts (**A**) and the nuclear protein extracts (**B**) of HUVECs in medium containing 5.5 (NG) or 30 mmol/L (HG) glucose for 48 h. **C** The localization of FOXO1. After being cultured in NG or HG for 48 h, HUVECs were subjected to H_2O_2 (300 μM for 30 min) and harvested at the indicated time points or left untreated. Scale bar, 20 μm. **D** Western blot analysis of FOXO1 and γH2AX. HUVECs were infected with Ads for *FOXO1* knockdown (sh-*FOXO1*) or vehicle controls (sh-ctrl) and then cultured in NG or HG for 48 h. **E** Western blot analysis of γH2AX. After being infected with Ads and then cultured in NG or HG for 48 h, HUVECs were subjected to H_2O_2 (300 μM for 30 min) and harvested at the indicated time points. **F** Confocal analysis of γH2AX foci. After being infected with Ads and cultured in NG or HG for 48 h, HUVECs were subjected to H_2O_2 (300 μM for 30 min, 2 h recovery), or left untreated. Scale bar, 10 μm. **G** and **H** DNA damage levels examined by comet assay. After the Ads infection and the following 48 h culture in NG or HG medium, HUVECs were subjected to H_2O_2 (300 μM for 30 min, 2 h recovery). Representative images (**G**, scale bar: 100 μm) and the scatter dot plot of the tail moment per cell (**H**) are shown. **I** and **J** Cellular senescence detected by SA-β-Gal staining. After being treated with H_2O_2 (700 μM for 30 min), HUVECs were infected with the indicated Ads and then cultured in NG or HG for 48 h. Scale bar, 100 μm. Each experiment was repeated independently at least three times. All results are displayed as means ± SD. $^*P < 0.05$, $^{**}P < 0.01$, $^{***}P < 0.001$, $^{****}P < 0.0001$, one-way ANOVA analysis.

treatment of inhibitors for these three kinases. The results of the comet assay showed that the decline of the tail moment by *FOXO1* knockdown was abrogated upon ATM inhibition, while neither ATR inhibitor nor DNA-PK inhibitor affected it, suggesting that *FOXO1* knockdown enhanced DNA repair via the ATM-dependent pathway (Fig. 3C and D, and Fig. S2B). As ATM relies on the MRN complex as both its activators and downstream targets [30], we next hypothesized that *FOXO1* knockdown altered the level of ATM and MRN. This was confirmed by Western blot showing that high glucose decreased the levels of ATM and MRN, which were improved by *FOXO1* knockdown with and without H_2O_2 treatment (Fig. 3E–H) whereas ATM inhibitors blocked these effects (Fig. 3I and J). We also detected the protein levels of some kinases

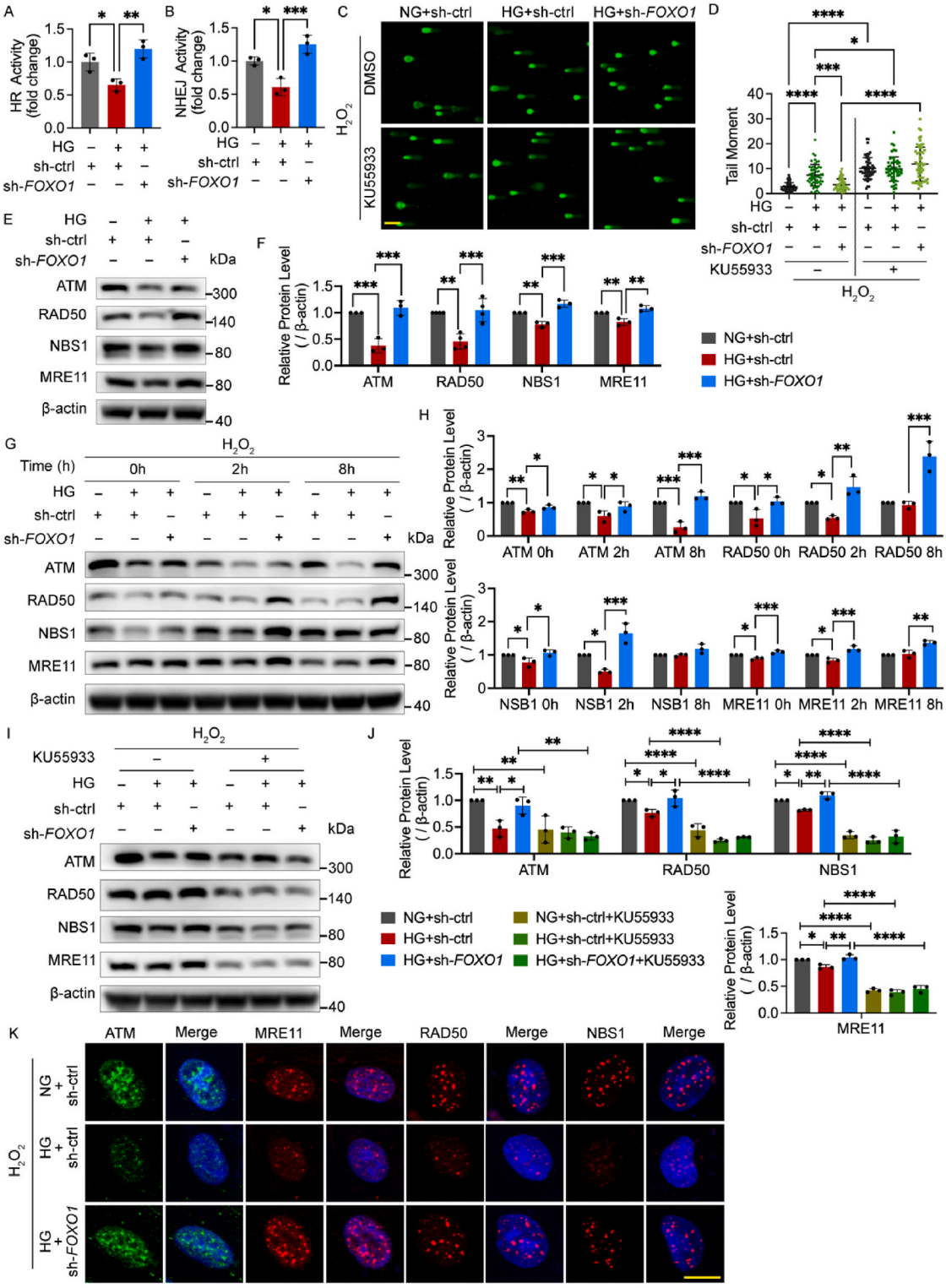

Fig. 3. *FOXO1* knockdown alleviates oxidative stress-induced DNA damage by enhancing DNA repair mediated by the MRN-ATM pathway. **A** and **B** HR and NHEJ activity. After being treated with DNA repair reporter (DRR) assay, HUVECs were infected with sh-*FOXO1* or sh-ctrl and then cultured in NG or HG for 48 h. **C** and **D** DNA damage levels assessed using comet assay. After being infected with sh-*FOXO1* or sh-ctrl, HUVECs were treated with DMSO or 15 μM of ATM inhibitor KU55933 for 48 h in NG or HG, and then subjected to H_2O_2 (300 μM for 30 min, 2 h recovery). The representative images (**C**, scale bar: 100 μm) and the scatter dot plot of the tail moment per cell (**D**) are shown. **E**-**J** Western blot analysis of ATM and MRN. HUVECs in (**E**) and (**F**) were infected with sh-*FOXO1* or sh-ctrl and then cultured in NG or HG for 48 h. HUVECs in (**G**) and (**H**) were treated with H_2O_2 (300 μM for 30 min) and harvested at the indicated time points after being infected with Ads and being cultured in NG or HG for 48 h. HUVECs in (**I**) and (**J**) were treated in the same conditions as (**C**) and (**D**). **K** Confocal analysis of ATM and MRN foci. After the Ads infection and the following 48 h culture in NG or HG, HUVECs were subjected to H_2O_2 (300 μM for 30 min, 2 h recovery). Scale bar, 10 μm. Each experiment was repeated independently at least three times. All results are displayed as means ± SD. $^*P < 0.05$, $^{**}P < 0.01$, $^{***}P < 0.001$, $^{****}P < 0.0001$, one-way ANOVA analysis.

involved in other DSBR pathways but found no measurable change, which was in line with the result of the comet assay (Fig. S2C). Next, the number of nuclear foci that represent the recruitment of kinases to the DNA damage sites was measured through immunofluorescence. Compared with the control group, high glucose decreased the foci number of ATM and MRN during the recovery from H_2O_2 treatment, which was improved by *FOXO1* knockdown (Fig. 3K).

The results above underscore that *FOXO1* knockdown alleviated oxidative stress-induced DNA damage under high glucose by enhancing DNA repair function mediated by the MRN-ATM pathway in HUVECs.

2.4. FOXO1 knockdown improves impaired metabolic capacity of glycolysis and mitochondrial respiration under high glucose

To investigate whether and how high glucose and *FOXO1* knockdown affect the glucose metabolism in ECs, the Real-Time ATP Rate Kit was used to determine the general metabolic phenotype by measuring the glycolysis-derived ATP (glycoATP), mitochondrial ATP (mitoATP), and total ATP production rate (Fig. 4A and B). High glucose impaired the glycoATP and mitoATP production rate under H_2O_2 stimulation, indicating an impairment of energy production under oxidative stress, while *FOXO1* knockdown increased both glycoATP and mitoATP production rates with and without H_2O_2 treatment. Moreover, all groups had more glycoATP production than mitoATP production rate, which is consistent with previous studies [31,32].

The intracellular ATP and lactate-to-pyruvate ratio were also measured to confirm this metabolic phenotype (Figs. S3A and B). Consistent with the result from the Real-Time ATP Rate Kit, high glucose decreased the ATP level under H_2O_2 treatment, while *FOXO1* knockdown increased ATP production with and without H_2O_2 treatment. The lactate-to-pyruvate ratio in the control group significantly increased after H_2O_2 treatment, suggesting a shift of glucose metabolism toward glycolysis for more ATP supply to overcome energy shortage. However, high glucose decreased the lactate-to-pyruvate ratio under H_2O_2 treatment, indicating that high glucose affected glycolytic mobilization. Meanwhile, *FOXO1* knockdown elevated the lactate-to-pyruvate ratio with and without H_2O_2 treatment, in synchrony with the ATP level. The intracellular NAD pool is a key metabolic component in glucose metabolism and exerts a critical role in boosting DNA damage repair [33]. As shown in Fig. S3C, high glucose decreased the intracellular NAD pool while FOXO1 knockdown elevated that.

Therefore, *FOXO1* knockdown improves the impaired metabolic capacity of both glycolysis and mitochondrial respiration under high glucose and glycolysis is the primary source of ATP production in ECs.

2.5. FOXO1 knockdown promotes DNA repair mediated by the MRN-ATM pathway independent of the mitochondrial function

Endothelial mitochondria are closely related to ROS generation and are considered the sensors and initiators of EC death [34]. To confirm the impact of *FOXO1* knockdown on mitochondrial respiration, HUVECs were subjected to the Mito Stress Test Kit. High glucose impaired the spare respiratory capacity with or without H_2O_2 treatment. *FOXO1* knockdown increased the spare respiratory capacity without H_2O_2 treatment and further elevated basal and spare respiratory capacities after the stimulation of H_2O_2 treatment (Fig. 4C and D). To investigate if the enhancement of mitochondrial respiration by *FOXO1* knockdown affects DNA damage and repair, the comet assay and Western blot for ATM and MRN were conducted after the treatment of mitochondrial electron transport chain inhibitors rotenone/antimycin (ROT/AA) or mitochondrial protonophore uncoupler BAM15 or FCCP. The mitochondrial electron transport chain inhibition did not block the effects of *FOXO1* knockdown on the oxidative DNA damage (Fig. 4E and F) and the MRN-ATM pathway (Fig. 4G) under high glucose. Moreover, the mitochondrial protonophore uncoupler neither alleviated oxidative DNA damage (Fig. 4H and I) nor significantly activated the MRN-ATM pathway (Fig. 4J). SA-β-Gal staining further showed that the mitochondrial electron transport chain inhibition did not block the protective effects of *FOXO1* knockdown on cellular senescence but led to a certain increase in SA-β-Gal activity of both the control group and *FOXO1* knockdown group (Fig. S3D). Therefore, mitochondrial dysfunction may play a role in cellular senescence through mechanisms other than direct inhibition of the MRN-ATM pathway, for example maintaining ongoing aberrant DNA damage responses by inducing ROS, as reported in a previous study [35].

2.6. FOXO1 knockdown enhances DNA repair mediated by the MRN-ATM pathway in a glycolysis-dependent manner

The above metabolic data provided a strong hint that the mobilization of glycolysis is critical for the energy supply in ECs to overcome oxidative stress. Therefore, the Glycolysis Rate Kit was used next to determine the impact of *FOXO1* knockdown on glycolysis. Under the stress of H_2O_2 treatment, high glucose impeded the HUVECs' basal glycolysis, which was not mobilized and led to a lower glycoPER-to-mitoOCR ratio. Meanwhile, *FOXO1* knockdown increased basal and compensatory glycolysis, as well as the glycoPER-to-mitoOCR ratio under high glucose with and without H_2O_2 treatment (Fig. 5A and B). The comparison between glycolysis with and without H_2O_2 treatment further illustrated the importance of glycolytic mobilization in response to oxidative stress, showing that after H_2O_2 treatment, basal and compensatory glycolysis leveled up in both the control group and *FOXO1* knockdown group but failed to increase in the high glucose group, suggesting either an impairment of glycolysis capacity under high glucose or a high level of oxidative stress under high glucose that cannot be further significantly increased by H_2O_2 (Figs. S4A and B).

The HUVECs were then subjected to the inhibition of glycolysis with 2DG to investigate whether glycolysis influenced DNA repair. Comet assay and Western blot for ATM and MRN showed that glycolysis inhibition increased the tail moment in all three groups, which hindered the effect of *FOXO1* knockdown accompanied by a decrease in the protein level of ATM and MRN (Fig. 5C–F). We also used the PFKFB3 inhibitor KAN0438757, another confirmed inhibitor of glycolysis in ECs [36], to further testify to the impact of glycolysis. The results of the comet assay showed that the PFKFB3 inhibitor also eliminated the effect of *FOXO1* knockdown (Fig. 5G and H).

2.7. FOXO1 knockdown improves DNA repair mediated by the MRN-ATM pathway via PFKFB3 activation

As the inhibition of glycolysis impaired DNA repair, we next measured the level of PFKFB3 and three glycolytic rate-limiting enzymes, namely, hexokinase, pyruvate kinase (PKM), and phosphofructokinase (PFK), to determine which enzyme may be involved in the effects of *FOXO1* knockdown on glycolysis and DNA repair. *FOXO1* knockdown elevated both the mRNA amount and protein level of PFKFB3, but no change was found for hexokinase, PFK, and PKM (Figs. S5A–C), indicating that PFKFB3 may be involved in the effect of *FOXO1* knockdown.

Next, we measured the protein level of PFKFB3 under oxidative stress. High glucose decreased the protein level of PFKFB3, which was reversed by the *FOXO1* knockdown (Fig. 6A and B). Afterward, immunofluorescence microscopy was conducted to illustrate the distribution of PFKFB3. The results indicated that PFKFB3 was distributed in the nuclei and plasma at the same time but show an obvious cluster around the nuclei in ECs (Fig. S5D), which is consistent with a previous study [31]. However, after H_2O_2 treatment, PFKFB3 translocated into the nuclei in the control group and the *FOXO1* knockdown group but still clustered in the perinuclear cytosol in the high glucose group (Fig. S5E), suggesting that FOXO1 may influence the subcellular location of PFKFB3, in addition to its protein level. The nuclear translocation of PFKFB3 after H_2O_2 treatment also hinted that PFKFB3 might be directly

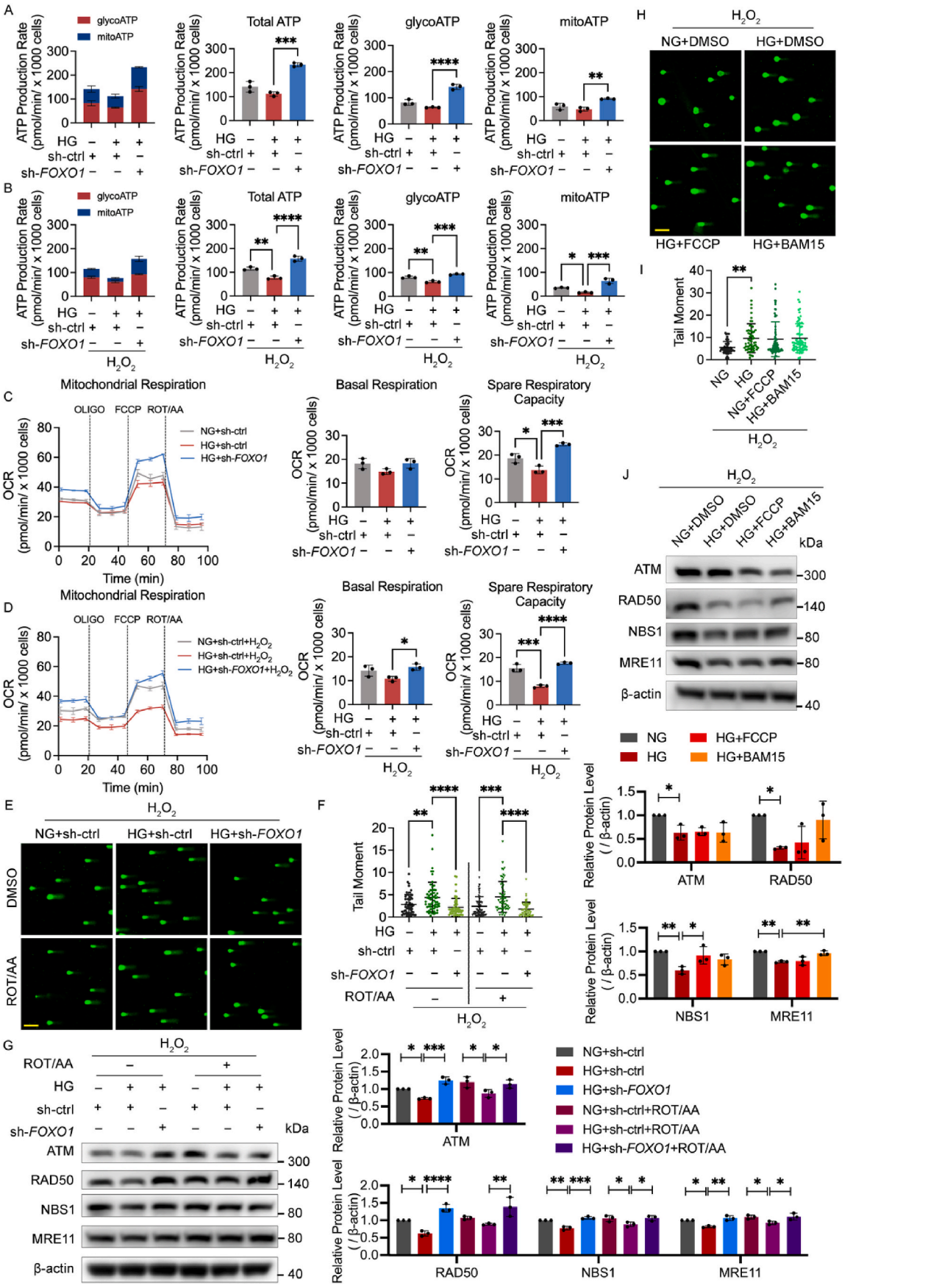

(caption on next page)

Fig. 4. *FOXO1* knockdown promotes DNA repair mediated by the MRN-ATM pathway independent of the mitochondrial function. **A-B** ATP production rate detected by Real-Time ATP Rate Kit. After being infected with sh-*FOXO1* or sh-ctrl and then cultured in NG or HG for 48 h, HUVECs were subjected to H_2O_2 (**B**, 300 μM for 30 min, 2 h recovery), or left untreated (**A**). Then, the ECAR and OCR were measured sequentially under basal conditions, following treatments of ATP synthase inhibitor Oligomycin (1.5 μM) and complex I/III inhibitors Rotenone/antimycin A (0.5 μM) and converted as ATP production rate. ATP production profiles, changes in glycolysis-derived ATP (glycoATP), mitochondrial ATP (mitoATP) and total ATP production are shown as indicated. **C-D** Mitochondrial respiration detected by Mito Stress Test. After being infected with sh-*FOXO1* or sh-ctrl and cultured in NG or HG for 48 h, HUVECs were subjected to H_2O_2 (**D**, 300 μM for 30 min, 2 h recovery), or left untreated (**C**). Then, the OCR was measured sequentially under basal conditions, following treatments of ATP synthase inhibitor Oligomycin (OLIGO, 1.5 μM), mitochondrial protonophore uncoupler FCCP (1 μM) and complex I/III inhibitors Rotenone/antimycin A (ROT/AA, 0.5 μM). OCR profiles, changes in basal respiration and spare respiratory rate are shown as indicated. **E-G** DNA damage levels in comet assay and western blotting analysis of ATM and MRN. After being infected with the indicated Ads, HUVECs were treated with DMSO or 0.5 μM of ROT/AA in NG or HG for 48 h and then subjected to H_2O_2 (300 μM for 30 min, 2 h recovery). **H-J** DNA damage levels in comet assay and western blotting analysis of ATM and MRN. HUVECs were treated with DMSO or 1 μM of BAM15 or FCCP in NG or HG for 48 h, and then subjected to H_2O_2 (300 μM for 30 min, 2 h recovery). Scale bar in (**E**) and (**H**), 100 μm. Each experiment was repeated independently at least three times. All results are displayed as means ± SD. $^*P < 0.05$, $^{**}P < 0.01$, $^{***}P < 0.001$, $^{****}P < 0.0001$, one-way ANOVA analysis.

involved in DNA repair within the nuclei of ECs in response to oxidative stress. To elucidate the role of PFKFB3 in DNA repair in greater detail, we assessed the co-localization of PFKFB3 foci with γH2AX and ATM foci upon the induction of H_2O_2. The results of immunofluorescence microscopy after the removal of the cytoplasm showed that PFKFB3 had a strong co-localization with the γH2AX and ATM foci (Fig. 6C), indicating that PFKFB3 translocated to oxidative stress-induced DSB sites and played a part in the DSBR function of the MRN-ATM pathway.

Therefore, we hypothesized that *PFKFB3* knockdown would disrupt DNA repair activity upon being subjected to oxidative stress and lead to unrepaired DSBs. The comet assay showed that *PFKFB3* knockdown markedly increased the tail moment of all three groups (Fig. 6D and E). SA-β-Gal staining also showed that *PFKFB3* knockdown significantly increased cellular senescence with and without H_2O_2 treatment (Fig. 6F and G, and Figs. S6A and B). Both results manifested that *FOXO1* knockdown alleviates DNA damage and cellular senescence in a PFKFB3-dependent manner. Next, the DRR assay was conducted to directly determine whether PFKFB3 participates in the improvement of DNA repair by *FOXO1* knockdown. The improvement of HR and NHEJ activity by *FOXO1* knockdown was abolished by *PFKFB3* knockdown (Fig. 6H and I). To elucidate the signaling pathways modulated by PFKFB3, we next measured the protein levels of ATM and MRN, showing that *PFKFB3* knockdown decreased the protein level of ATM and MRN in all three groups and eliminated the effects of *FOXO1* knockdown (Fig. 6J and K). Furthermore, in the immunofluorescence microscopy, *PFKFB3* knockdown decreased the foci numbers of ATM and MRN with an increase of γH2AX foci (Fig. 6L), indicating unrepaired DSBs accompanied by defective DSBR under oxidative stress.

2.8. PFKFB3 overexpression restores impaired DNA repair in response to oxidative stress under high glucose by interaction with the MRN-ATM pathway

Adenoviruses for *PFKFB3* overexpression were utilized next to confirm whether *PFKFB3* overexpression attenuates DNA damage by improving DNA repair. *PFKFB3* overexpression decreased the protein level of γH2AX with and without H_2O_2 treatment (Fig. 7A–D) and reduced the comet tail moment under high glucose (Fig. 7E and F), and the SA-β-Gal staining results showed that *PFKFB3* overexpression also alleviated cellular senescence under high glucose with and without H_2O_2 treatment (Fig. 7G and H, and Figs. S6C and D).

Then, Western blot for ATM and MRN and DRR assay were conducted to further confirm the role of PFKFB3 in DNA repair. *PFKFB3* overexpression increased the protein levels of ATM and MRN together with the decline of γH2AX (Fig. 7C and D) and enhanced the HR and NHEJ activities under high glucose (Fig. 7I and J). Coimmunoprecipitation was conducted to confirm the direct interaction between ATM, MRN and PFKFB3, showing that PFKFB3 interacted with ATM and MRN during the recovery from H_2O_2 treatment (Fig. 7K). Immunofluorescence microscopy further illustrated that the foci numbers of ATM and MRN were elevated by *PFKFB3* overexpression with the alleviation of γH2AX foci under high glucose (Fig. 7L) while ATM inhibition blocked the formation of the PFKFB3 foci and the co-localization of PFKFB3 and ATM (Fig. S6E). These results suggested the existence of an interactive feedback between PFKFB3 and DNA damage response signals. Moreover, consistent with the effects of *FOXO1* knockdown, *PFKFB3* overexpression increased the intracellular NAD pool of HUVECs under high glucose (Fig. S6F), indicating a possible metabolic regulation by PFKFB3 on DNA repair.

2.9. Pfkfb3 overexpression attenuates oxidative stress damage in diabetic mouse retina

To investigate the state of PFKFB3 in vivo, we analyzed the PFKFB3 protein level in the retinas of diabetic mice (Fig. 8A). The results showed that PFKFB3 decreased in diabetic retina, but *Foxo1* knockdown restored it. The decline in *PFKFB3* expression was also confirmed in the retinal fibrovascular membrane of diabetic patients compared with that of the macular epiretinal membrane of non-diabetic patients, as shown in the results of qPCR and immunofluorescence staining (Fig. 8B and C). The intravitreal injection of adenovirus for *Pfkfb3* overexpression was conducted next to confirm the effect of PFKFB3 in vivo. We determined the protein level and foci number of γH2AX, showing that *Pfkfb3* overexpression alleviated γH2AX accumulation in the retinas of diabetic mice (Fig. 8D and E). EB assays and retinal trypsin digestion assays were next conducted to assess the vascular dysfunction, showing that the increased retinal vascular leakage and acellular capillary number in the retinas of diabetic mice were decreased by *Pfkfb3* overexpression (Fig. 8F–I). Given these results, *Pfkfb3* overexpression attenuated diabetes-induced retinal DNA damage and vascular dysfunction in vivo.

3. Discussion

In the present study, we propose a pathological model where the impairment of DNA repair driven by aberrant glycolysis is a critical trigger for hyperglycemia-induced endothelial oxidative DNA damage and vascular dysfunction. Persistent oxidative stress-induced DNA damage is a crucial pathological factor for the development of diabetic vascular complications [4,5,37] and higher radiosensitivity has been observed in the microvasculature of patients with diabetes [38–40]. Our study determined impaired glycolysis-dependent DNA repair as a key factor in persistent oxidative stress injury of diabetic ECs. It has been reported that enhanced glycolysis confers radio-resistance by facilitating DNA repair in tumor cells [41,42] and diabetic patients have a higher risk for cancer in virtually any site [43,44]. Moreover, recent evidence has shown that high glucose also impedes DNA repair in mesangial cells and hepatocytes and restoring DNA repair reduces diabetes-related pulmonary and renal fibrosis [10,11,45]. Those reports signify that the interaction between metabolic reprogramming and maladaptive DNA repair may be a unifying model for multisystemic diabetic complications.

FOXO1 is stimulated by various damaging triggers under hyperglycemia, including oxidative and genotoxic stress. Oxidative stress leads to the activation of SIRT1 that deacetylates FOXO1, causing its nuclear

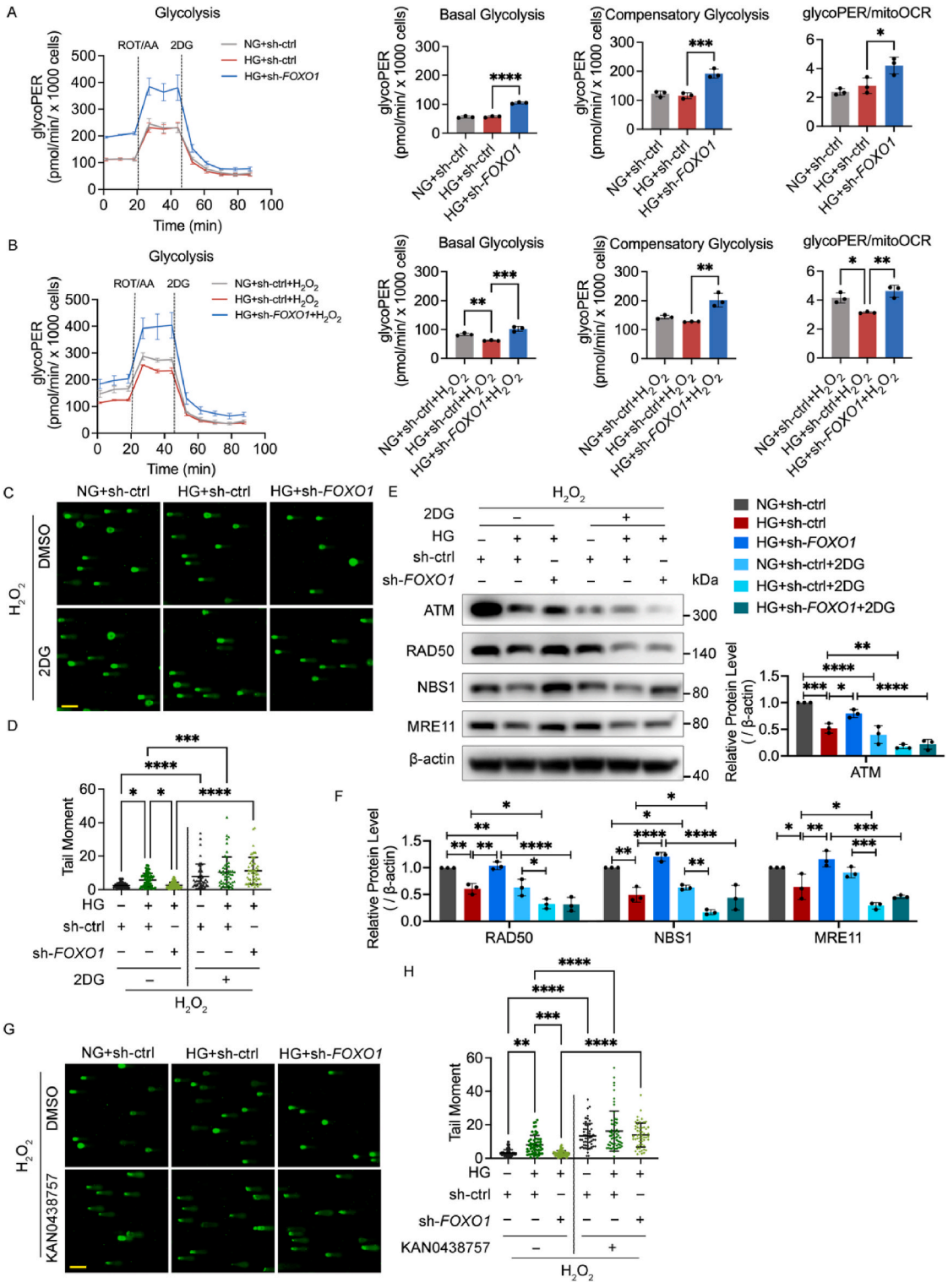

Fig. 5. *FOXO1* knockdown enhances DNA repair mediated by the MRN-ATM pathway in a glycolysis-dependent manner. **A** and **B** Glycolysis detected by Glycolysis Rate Kit. After being infected with sh-*FOXO1* or sh-ctrl and then cultured in NG or HG for 48 h, HUVECs were subjected to H_2O_2 (**B**, 300 μM for 30 min, 2 h recovery), or left untreated (**A**). The ECAR and OCR were measured sequentially under basal conditions, following treatments of ROT/AA (0.5 μM) and 2-deoxy-glucose (2DG, 50 mM), and converted as glycolytic proton efflux rate (glycoPER) and mitochondrial oxygen consumption rate (mitoOCR). GlycoPER profiles, changes in basal glycolysis, compensatory glycolysis and glycoPER/mitoOCR are shown as indicated. **C** and **D** DNA damage levels assessed using comet assay. After being infected with sh-*FOXO1* or sh-ctrl, HUVECs were treated with DMSO or 50 mM of 2DG in NG or HG for 48 h, and then subjected to H_2O_2 (300 μM for 30 min, 2 h recovery). The representative images (**C**, scale bar: 100 μm) and the scatter dot plot of the tail moment per cell (**D**) are shown. **E** and **F** Western blot analysis of ATM and MRN. HUVECs were treated in the same conditions as (**C**) and (**D**). **G** and **H** DNA damage levels were assessed using comet assay. After being infected with sh-*FOXO1* or sh-ctrl, HUVECs were treated with DMSO or 25 μM of KAN0438757 in NG or HG for 48 h, and then subjected to H_2O_2 (300 μM for 30 min, 2 h recovery). The representative images (**G**, scale bar: 100 μm) and the scatter dot plot of the tail moment per cell (**H**) are shown. Each experiment was repeated independently at least three times. All results are displayed as means ± SD. $^{*}P < 0.05$, $^{**}P < 0.01$, $^{***}P < 0.001$, $^{****}P < 0.0001$, one-way ANOVA analysis.

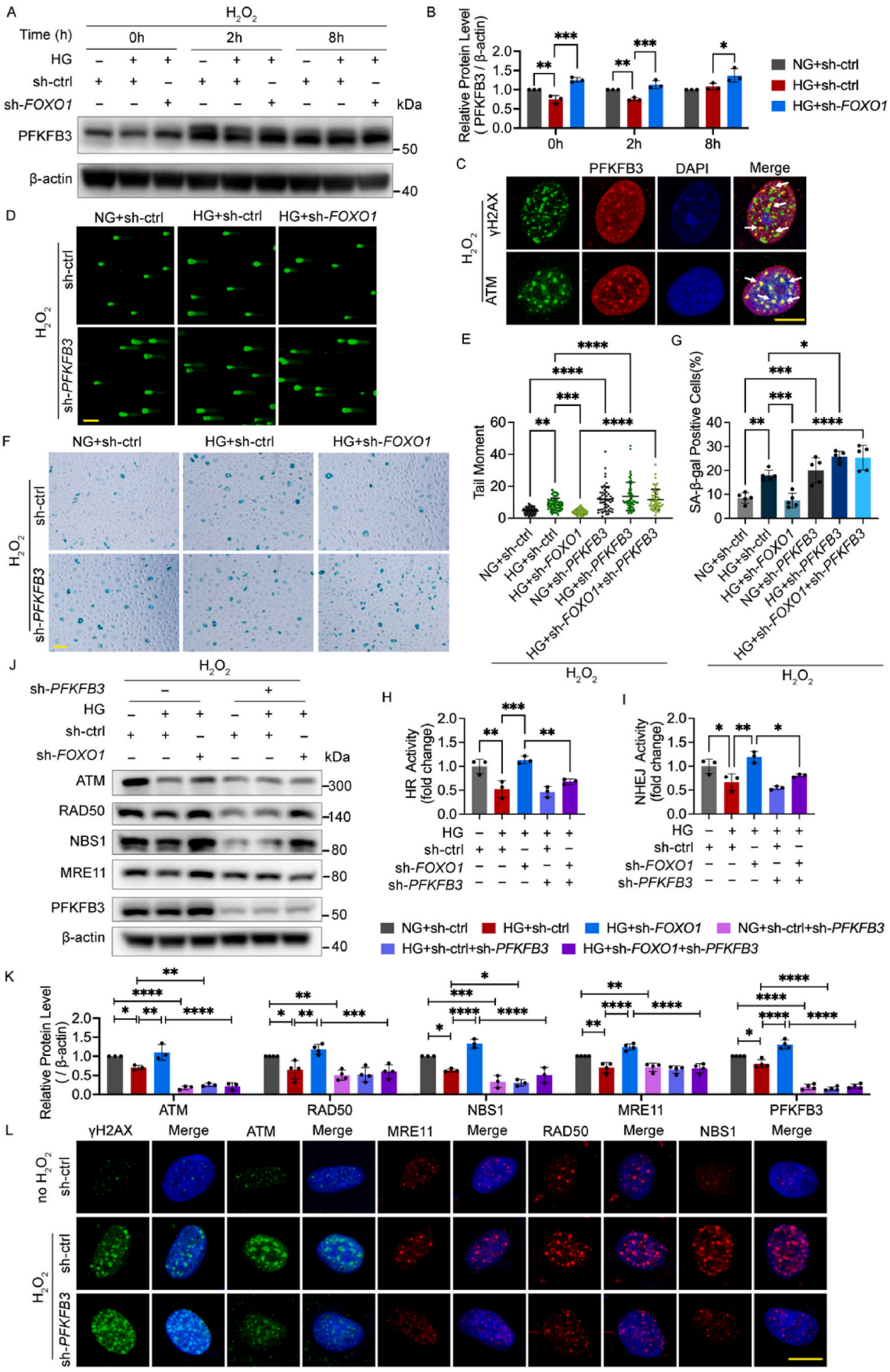

(caption on next page)

Fig. 6. *FOXO1* knockdown improves DNA repair mediated by the MRN-ATM pathway via PFKFB3 activation. **A** and **B** Western blot analysis of PFKFB3. After being infected with sh-*FOXO1* or sh-ctrl and then cultured in NG or HG for 48 h, HUVECs were subjected to H_2O_2 (300 μM for 30 min) and harvested at the indicated time points. **C** Confocal analysis of the recruitment of PFKFB3 to DNA damage sites γH2AX foci and the colocalization between PFKFB3 and ATM in HUVECs upon H_2O_2 (300 μM for 30 min, 2 h recovery). White arrows indicate co-localized foci. Scale bar, 10 μm. **D** and **E** DNA damage levels assessed by comet assay. After being infected with Ads for *PFKFB3* knockdown (sh-*PFKFB3*), sh-*FOXO1* or sh-ctrl and then cultured in NG or HG for 48 h, HUVECs were subjected to H_2O_2 (300 μM for 30 min, 2 h recovery). The representative images (**D**, scale bar: 100 μm) and the scatter dot plot of the tail moment per cell (**E**) are shown. **F** and **G** Cellular senescence in HUVECs. After being treated with H_2O_2 (700 μM for 30 min), HUVECs were infected with the indicated Ads and then cultured in NG or HG for 48 h. Scale bar, 100 μm. **H** and **I** HR and NHEJ activity. After being treated with DNA repair reporter (DRR) assay, HUVECs were infected with Ads and then cultured in NG or HG for 48 h. **J** and **K** Western blotting analysis of ATM, MRN and PFKFB3. HUVECs were treated in the same conditions as (**D**) and (**E**). **L** Confocal analysis of γH2AX, ATM and MRN foci. After being infected with sh-*PFKFB3* or sh-ctrl for 48 h, HUVECs were subjected to H_2O_2 (300 μM for 30 min, 2 h recovery), or left untreated. Scale bar, 10 μm. Each experiment was repeated independently at least three times. All results are displayed as means ± SD. $^*P < 0.05$, $^{**}P < 0.01$, $^{***}P < 0.001$, $^{****}P < 0.0001$, one-way ANOVA analysis.

trapping and increasing its transcriptional activity [25,46,47]. Genotoxic stress reduces the phosphorylation of FOXO1 by CDK2, which also results in its nuclear localization [48–51]. FOXO1 can also be activated by inflammatory factors TNF-α and induce cascading inflammatory responses [18,25,52] and persistent DNA damage itself can promote inflammation as well as ROS [53]. Our study exposed ECs to oxidative and genotoxic stress through both the high glucose and H_2O_2 treatment. We observed how FOXO1 overactivation under high glucose impeded the necessary interaction of DNA repair and glycolysis, and more importantly, we elucidated how preserved glycolysis-dependent DNA repair under high glucose by *FOXO1* knockdown operated timely to cope with endothelial oxidative damage, which helps to comprehensively discern the role of metabolic abnormality in the DNA repair disability in diabetic ECs.

Although FOXO1 helps maintain the quiescent state of ECs in most healthy tissues by reducing glycolysis [24], our data showed that healthy ECs after H_2O_2 treatment have a metabolic divert to glycolysis to support timely DNA repair responses, but ECs under hyperglycemia failed to mobilize glycolysis due to the hyperactivation of FOXO1, with concomitant impairment of DNA repair. We also determined abnormal glycolysis as the primary culprit of impaired DNA repair, although *FOXO1* knockdown enhanced both glycolysis and oxidative phosphorylation. Consistent with that, an aberrant relative metabolic shift from glycolysis to oxidative phosphorylation under metabolic and oxidative stress has also been identified in diabetic retinas [54–56] and endothelial-specific FOXO1 depletion contributes to a prevention of obesity-related disorders by increasing endothelial proliferative and glycolytic capacities [57]. Intriguingly, the cardiomyocyte-specific deletion of *Foxo1* also rescues diabetic cardiac dysfunction via a shift in the metabolic substrate usage to glucose [19] and FOXO1 inhibition alleviates diabetes-related diastolic dysfunction by increasing myocardial pyruvate dehydrogenase activity and glucose tolerance [20], indicating a common role of inhibited glycolysis by FOXO1 for diabetic cardiovascular complications.

PFKFB3 is a key regulatory enzyme of glycolysis by synthesizing and degrading fructose-2,6-bisphosphate, an allosteric activator for the rate-limiting enzyme PFK [31]. PFKFB3 regulates EC proliferation and vessel sprouting by controlling the formation of filopodia/lamellipodia and directional migration [31,32], which reveals the remarkable significance of the link between metabolism and EC function. PFKFB3 has been linked to the malignancy of tumor cells via enhancing glycolysis in the cytoplasm [58,59] as well as via facilitating DNA repair with its nuclear form [60,61]. Similar to the Warburg effect in tumor cells, healthy ECs produce ATP mainly by aerobic glycolysis [31,32] while in senescent ECs PFKFB3 is significantly downregulated, leading to a decline of glycolysis and glucose tolerance [62]. Our results confirmed that *PFKFB3* knockdown aggravated cellular senescence, while *PFKFB3* overexpression alleviated cellular senescence by increasing the defensive capability from DNA damage in diabetic ECs. Cardiomyocytes under high glucose have also been reported to have a lower level of PFKFB3, which reduces glucose metabolism and results in susceptibility to hyperglycemia [63], indicating a common pathological model related to the inhibition of PFKFB3 for diabetic cardiovascular complications.

As previously reported [14,64,65], impaired DNA repair involving the MRN-ATM pathway is a potential therapeutic target for diabetic complications. Our results showed that PFKFB3 directly relocated to the DSB foci in response to oxidative stress and is indispensable for the activation of the MRN-ATM pathway. Moreover, ATM inhibitor blocked the PFKFB3 recruitment to DNA damage sites, suggesting that PFKFB3 can also promote DNA repair downstream of ATM. Therefore, oxidative stress-induced DSBs initiate cascade-amplified DNA repair responses through a positive-feedback loop consisting of MRN, ATM, γH2AX, as well as PFKFB3. Defects in any step would hamper the complex system consisting of DNA damage response and DSBR signaling.

Our study focused on the relation of DNA repair with the general level of glycolysis. But glycolysis is fluxed into four damaging pathways with a variation in numerous metabolic components under hyperglycemia. The conversion of sorbitol in the polyol pathway to fructose and the activation of PARP can drain intracellular NAD pool [66], impairing DSBR activity and causing cellular senescence [67]. Our results showed that both *FOXO1* knockdown and *PFKFB3* overexpression increased the intracellular NAD pool, and a previous study has reported that a small-molecule PFKFB3 inhibitor 3PO suppresses glucose uptake and decreases the intracellular concentration of NAD + and NADH [68]. Therefore, future studies need to address whether these pathways impair DNA repair or are mechanistically related to FOXO1 or PFKFB3. We have discussed the role of preserved DNA repair in the onset of early DR. A recent study also revealed that the elimination of the senescent subsets of ECs yields physiological vascular repair in the mouse model of oxygen-induced retinopathy [69]. Taking these into account, whether the improvement of DNA repair and the alleviation of endothelial senescence by the knockdown of *FOXO1* or overexpression of *PFKFB3* could be beneficial to retinopathy with pathological angiogenesis remains to be studied.

Collectively, our study proposed that metabolic reprogramming under hyperglycemia compromised genomic stability not only by inducing oxidative stress but also by impairing glycolysis-dependent DNA repair. In such a case, the inhibition of FOXO1 and supplement of PFKFB3 could be novel protective approaches for diabetic vascular complications due to their potential to promote oxidative DNA damage repair in diabetic ECs. With our findings in mind, the interaction of metabolic reprogramming and defective DNA repair should inspire the future development of therapies against diabetic vascular complications.

4. Methods

4.1. Adenoviruses

Adenoviruses (Ads) sh-*Foxo1*, sh-*FOXO1*, and sh-*PFKFB3* expressing short hairpin RNAs targeting mouse *Foxo1* mRNA, human *FOXO1* mRNA, or human *PFKFB3* mRNA; ad-*Pfkfb3* and ad-*PFKFB3* overexpressing mouse *Pfkfb3* mRNA (GenBank NM_001177752) or human *PFKFB3* mRNA (GenBank NM_004566); and vehicle control sh-ctrl and ad-ctrl were purchased from OBiO Technology (Shanghai, China). The shRNAs were mixed before transfection. The knockdown target

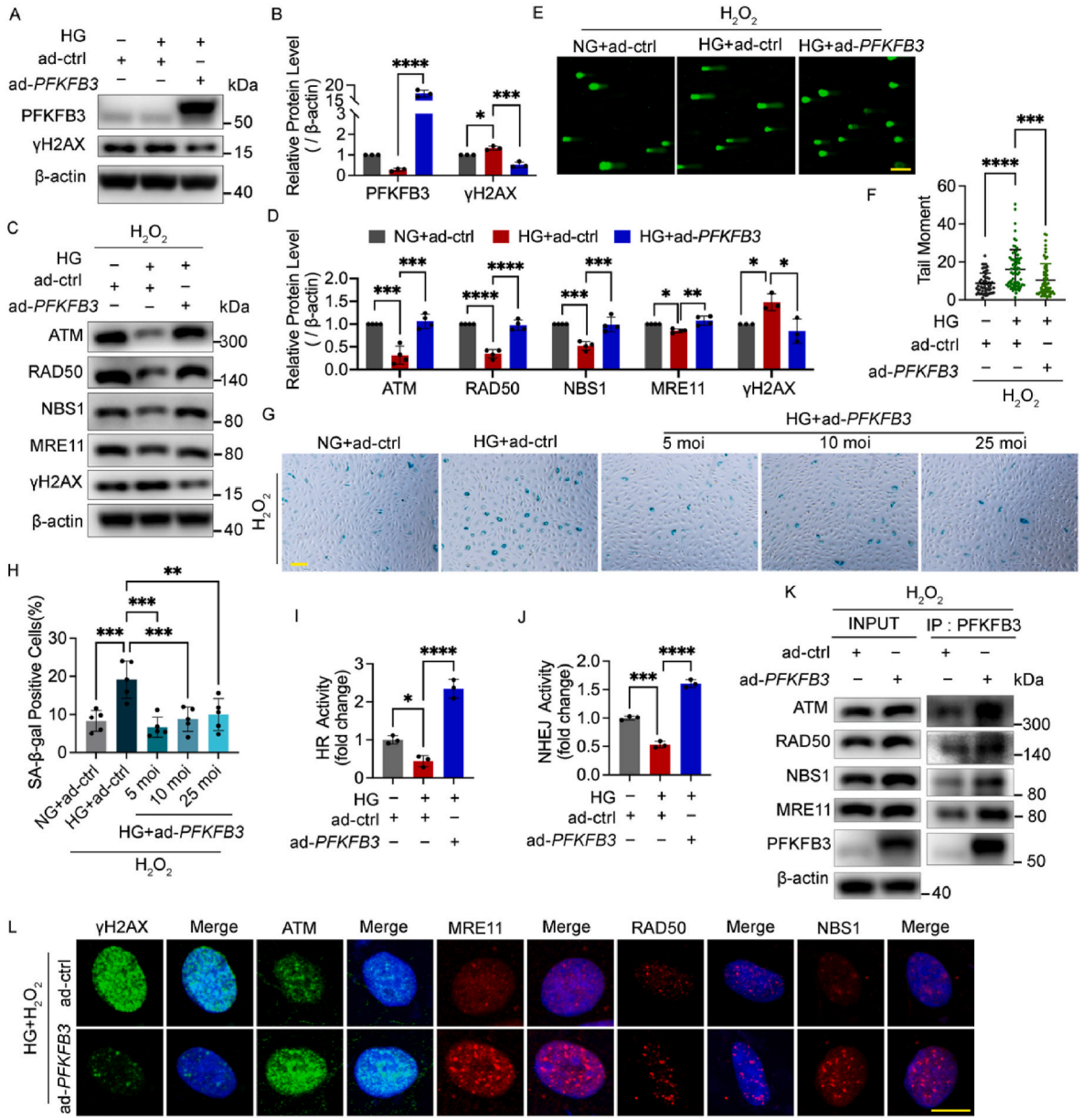

Fig. 7. *PFKFB3* overexpression restored impaired DNA repair in response to oxidative stress under high glucose by interaction with the MRN-ATM pathway. **A** and **B** Western blotting analysis of PFKFB3 and γH2AX. HUVECs were treated with Ads for *PFKFB3* overexpression (ad-*PFKFB3*) or vehicle control (ad-ctrl) and then cultured in NG or HG for 48 h. **C** and **D** Western blotting analysis of ATM and MRN. After being infected with ad-*PFKFB3* or ad-ctrl and then cultured in NG or HG for 48 h, HUVECs were subjected to H_2O_2 (300 μM for 30 min, 2 h recovery). **E** and **F** DNA damage levels assessed by comet assay. HUVECs were treated in the same conditions as (**C**) and (**D**). The representative images (**E**, scale bar: 100 μm) and the scatter dot plot of the tail moment per cell (**F**) are shown. **G** and **H** Cellular senescence detected by SA-β-Gal staining. After being treated with H_2O_2 (700 μM for 30 min), HUVECs were infected with Ads and then cultured in NG or HG for 48 h. Scale bar, 100 μm. **I** and **J** HR and NHEJ activity. After being treated with DNA repair reporter (DRR) assay, HUVECs were infected with Ads and then cultured in NG or HG for 48 h. **K** HUVECs were treated with ad-*PFKFB3* or ad-ctrl for 48 h as indicated, and then subjected to H_2O_2 (300 μM for 30 min, 2 h recovery). Cell lysates (left, INPUT) and immunoprecipitated PFKFB3 (right, IP: PFKFB3) was immunoblotted with ATM and MRN antibody. **L** Confocal analysis of γH2AX, ATM and MRN foci. After being infected with ad-*PFKFB3* or ad-ctrl and then cultured in HG for 48 h, HUVECs were subjected to H_2O_2 (300 μM for 30 min, 2 h recovery). Scale bar, 10 μm. Each experiment was repeated independently at least three times. All results are displayed as means ± SD. $^*P < 0.05$, $^{**}P < 0.01$, $^{***}P < 0.001$, $^{****}P < 0.0001$, one-way ANOVA analysis.

sequences are shown in Supplementary Table 1.

4.2. DR mouse model and intravitreal injection

Wild-type (WT) C57BL/6 male mice were purchased from the Shanghai Laboratory Animal Center, Chinese Academy of Sciences (Shanghai, China). The type 1 diabetic mouse model was induced by intraperitoneal injection of streptozotocin (STZ, Sigma Aldrich). Mice (8 weeks old, ~25 g body weight) were randomly assigned to the DR or WT group. The DR group was fasted for 12 h before the first STZ injection and then administered with STZ (55 mg/kg in 10 mM citrate buffer, pH 4.5) injection for 6 consecutive days. The WT group received sodium citrate buffer as vehicle control. All mice had free access to food and water in an air-conditioned room with a 12-h light–dark cycle. The mice with random blood glucose levels over 300 mg/dL were determined as diabetic mice, and then randomly assigned to different experimental groups, n = 6–12 for each group.

Two months after diabetic induction, the mice received two

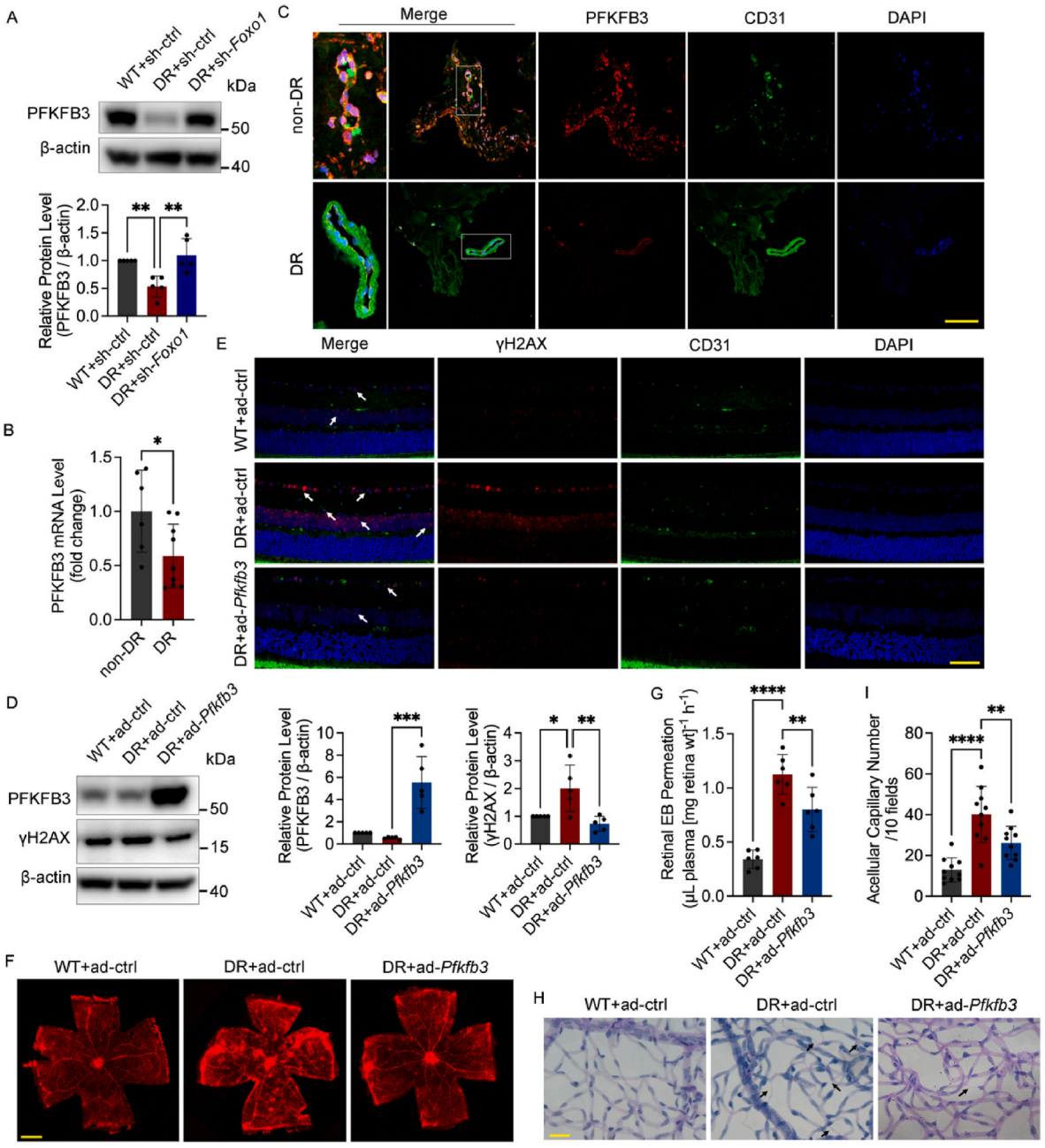

Fig. 8. *Pfkfb3* overexpression attenuates oxidative stress damage in diabetic mouse retina. **A** Western blot analysis of PFKFB3 in the whole retina extracts. Nondiabetic C57BL/6 mice (WT) and diabetic mice (DR) received the intravitreal injection of sh-*Foxo1*, or sh-ctrl as indicated. n = 10. **B** Human specimens include macular epiretinal membranes from patients without DR (non-DR, n = 6 eyes) and retinal fibrovascular membranes from patients with DR (DR, n = 9 eyes). qPCR was conducted to detect the expression of *PFKFB3*. **C** Immunofluorescence staining of PFKFB3 in macular epiretinal membranes from non-DR patients (n = 5 eyes) and retinal fibrovascular membranes (n = 6 eyes) from DR patients. Scale bar, 100 μm. **D** Western blot analysis of PFKFB3 and γH2AX. Nondiabetic C57BL/6 mice (WT) and diabetic mice (DR) received the intravitreal injection of Ads for *Pfkfb3* overexpression (ad-*Pfkfb3*), or vehicle controls (ad-ctrl) as indicated. n = 10. **E** Immunofluorescence staining of γH2AX. White arrows indicate γH2AX foci. n = 12. Scale bar, 50 μm. **F** and **G** Retinal vascular leakage assessed by EB dye. The confocal analysis of whole-mounted retinas (**F**, scale bar: 500 μm) and statistical results of spectrophotometrically measured EB extravasation (**G**) are shown. n = 12. **H** and **I** The number of acellular capillaries detected by retinal trypsin digestion. Scale bar, 20 μm. Black arrows indicate acellular capillaries. n = 10. All results are displayed as means ± SD. $^{*}P < 0.05$, $^{**}P < 0.01$, $^{***}P < 0.001$, $^{****}P < 0.0001$, for **B**, unpaired two-tailed Student's t-test, for **G** and **I**, one-way ANOVA analysis.

intravitreal injections of Ads at one and a half months' intervals. The mice were anesthetized with a 10:50 mix of ketamine (100 mg/mL) and xylazine (20 mg/mL) through intraperitoneal injection, following pupil dilation with 0.5% tropicamide phenylephrine drops and local anesthesia with 0.4% Benoxinate HCl drops (Santen Pharmaceuticals, Osaka, Japan). A 33-gauge disposable needle was passed through the sclera at the equator and posterior to the limbus into the vitreous cavity. A total of 1 μL Ads or vehicle controls were injected into the vitreous cavity with direct observation of the needle above the optic nerve head. The Ads were used in 1×10^{11} pfu/mL titers. The mice were euthanized by CO_2 inhalation, and their eyeballs were harvested ~5 months after diabetic induction.

4.3. Human archived pathological membrane tissues

Retinal fibrovascular membrane tissues harvested from patients with

DR and macular epiretinal membrane tissues harvested from patients without DR (non-DR) were used for blinded *PFKFB3* quantification through quantitative real-time PCR and immunofluorescence staining. The evaluation of DR was according to the International Clinical Diabetic Retinopathy Severity Scale adopted by the American Academy of Ophthalmology (AAO) and the International Council of Ophthalmology (ICO). The clinical information of the patients is included in Supplemental Table 2.

4.4. Cell culture

Human umbilical vein endothelial cells (HUVECs, at passage five or six) were purchased from ScienCell (California, USA) and cultured in an endothelial cell medium (ScienCell) supplemented with 5% fetal bovine serum, 1% ECGS, 100 U/mL penicillin, and 100 μg/mL streptomycin at 5.5 mmol/L D-glucose concentration for normal glucose and 30 mmol/L for high glucose. They were incubated at 37 °C in a humidified incubator containing 5% CO_2 with 95% relative humidity.

For Ad infection, the HUVECs were infected with sh-*FOXO1* or sh-*PFKFB3* at a multiplicity of infection (moi) of 100, ad-*PFKFB3* at 25 moi, or corresponding vehicle control at approximately 70% confluence and then cultured in normal or high glucose for 48 h. The small-molecule inhibitors and chemicals are used individually or in combination with adenoviruses during the culture for 48 h. For H_2O_2 treatment, HUVECs were incubated in 300 μM H_2O_2 for 30 min after the culture for 48 h to induce oxidative stress injury, except for the establishment of senescent phenotype described separately below. The small-molecule inhibitors and chemicals are shown in Supplemental Table 3.

4.5. Immunofluorescence staining

Eyeballs from mice or human tissues were fixed with 4% paraformaldehyde (PFA, Sangon Biotech, Shanghai, China) overnight at 4 °C. For the paraffin section, tissues were paraffin-embedded and sectioned at 5 μm thickness. The fixed eyeballs were sectioned through the optic disk. Before staining, the paraffin sections were dewaxed with xylene and rehydrated by sequential dipping into different concentrations of ethanol and water. Antigens were retrieved in a boiled target retrieval solution (Beyotime) for 15 min. For whole retina mounting, fixed mice retinas were isolated under an operating microscope and then permeabilized in PBS containing 1% Triton X-100 (Sigma Aldrich) at 25 °C for 30 min.

After three washes with PBS, the paraffin sections or whole retina mountings were blocked in a blocking buffer (PBS containing 5% BSA and 0.5% Triton X-100) for 30 min at 37 °C and incubated with primary antibody diluted in the blocking buffer at 4 °C overnight. Then, they were subjected to a secondary antibody diluted in the blocking buffer for 1 h at 25 °C. After each incubation, three washes with PBS were performed. For TUNEL staining, an In Situ Cell Death Detection Kit (Roche, Indianapolis, IN, USA) was used according to the manufacturer's instructions. Cell nuclei were stained with 4′,6-diamidino-2-phenylindole (DAPI). Images were taken with a confocal microscope (× 200 or × 400 magnification, Leica Microsystems, Wetzlar, Germany).

4.6. Evans blue assay

Retinal capillary permeability was determined through Evans blue (EB) staining. EB dye (Sigma Aldrich) was dissolved in PBS at a concentration of 25 mg/mL, sonicated for 5 min, and then filtered (pore size, 0.22 μm). The EB dye was injected through the tail vein at a dosage of 50 mg/kg over 10 s for 1 h circulation. For immunofluorescence observation, the eyes were collected and fixed in 4% PFA for 2 h at 25 °C. The retinas were then mounted on glass slides after being dissected and cut radically, and Z-stack images were captured with a confocal microscope (× 100 magnification). For quantitative assessment, the chest cavity was opened, and 0.2 ml of blood samples were collected. The eyes were enucleated after perfusion with citrate buffer (0.05 M, pH 3.5), and the retinas were dissected from the eyeballs and dried for 5 h. After the measurement of retinal dry weight, the EB dye was extracted with formamide (0.2 mL per retina, Sigma Aldrich) at 78 °C overnight and then centrifuged at 12,000 g at 4 °C for 15 min. The blood samples were centrifuged at 12,000 g at 4 °C for 15 min. The supernatants were spectrophotometrically detected for EB dye measurement by absorbance at 620 and 740 nm (background subtracted). The concentration of EB dye was calculated from a standard curve of EB dye in formamide. Retinal vascular leakage was calculated using the following equation: retinal EB dye (μg)/retinal dry weight (mg)/plasma EB concentration (μg/μL)/circulation time (h). Results were expressed in μL plasma × mg retinal wt^{-1} h^{-1}.

4.7. Retinal trypsin digestion assay

The number of acellular capillaries was assessed through a retinal trypsin digestion assay. The eyes were enucleated from the mice and fixed in 4% PFA for 24 h at 4 °C. The retinas were dissected and washed with water for 10 min, then incubated in 0.25% trypsin (Servicebio, Wuhan, China) for 12 h at 37 °C. When the tissue became loose, the vasculatures were isolated through gentle percussion and shaking. The retinal vasculatures were then mounted on glass slides and stained with periodic acid-Schiff and hematoxylin (Beyotime). The number of acellular capillaries was counted in 30 random fields per retina and averaged per 10 fields under a light microscope (× 630 magnification).

4.8. Western blot analysis

Cultured HUVECs or mouse retinal samples were lysed in RIPA lysis buffer (Cell signaling) containing 1 mM PMSF (Beyotime) and 1 × protease/phosphatase inhibitor cocktail (Roche). For the nuclear protein extraction, cells were lysed with the Nuclear and Cytoplasmic Protein Extraction Kit (Beyotime), as instructed in the manual. Protein concentrations were measured using a BCA protein assay reagent (Beyotime). Samples were loaded onto a 4–20% SDS-PAGE gel (30 μg/sample) at 180 V. For immunodetection, the gels were transferred onto Immuno-blot polyvinylidene fluoride membranes (Roche, pore size 0.22 μm) in the Trans-Blot Turbo Transfer System (Bio-Rad) and subsequently blocked in TBS-T (TBS + 0.1% Tween-20) with 5% nonfat milk powder at 37 °C for 3 h. Next, the membranes were immunoblotted with primary antibody diluted in a primary antibody dilution buffer (Beyotime) at 4 °C overnight. After three washes in TBS-T, the membrane was incubated for 1 h at 25 °C with peroxidase-conjugated secondary antibodies diluted in TBS-T with 1% nonfat milk powder. Antibody detection was performed with an enhanced chemiluminescence substrate (Millipore, Billerica, MA, USA). The antibodies used are shown in Supplemental Table 4.

4.9. Immunofluorescence microscopy

HUVECs were grown on eight-well slides (Millipore) and fixed with 4% PFA and 2% sucrose (Sigma Aldrich) for 10 min at 25 °C. They were then permeabilized with 0.5% Triton X-100 for 10 min at 25 °C, followed by a 30-min incubation in blocking buffer (Beyotime). The slides were subsequently incubated in primary antibody at 4 °C overnight and in secondary antibody for 1 h at 25 °C. The DNA was stained with DAPI at 25 °C for 10 min. The coverslips were mounted with antifade mounting medium (Beyotime). Images were acquired through confocal microscopy using a 20 × or 63 × oil immersion lens and processed in ImageJ or CellProfiler. The antibodies used are shown in Supplemental Table 4.

4.10. Nuclear fraction

To visualize stable PFKFB3, γH2AX, ATM, MRE11, RAD50, and NBS1

foci at the DNA damage sites induced by H_2O_2 treatment, the HUVECs grown on the slides were treated with nuclear fraction procedures to remove soluble cytoplasmic proteins and loosely held nuclear proteins, as previously described [60,70]. The HUVECs were first washed with PBS and then incubated for 3 min on ice in a cytoskeleton (CSK) buffer (pH 7.0) containing 10 mM PIPES (Sigma Aldrich), 100 mM NaCl (Sigma Aldrich), 300 mM sucrose, 3 mM $MgCl_2$ (Beyotime), 1 mM EGTA (Beyotime), and 0.7% Triton X-100. After the removal of the cytoplasm, the slides were washed three times with PBS and treated with the procedures of immunofluorescence microscopy.

4.11. Coimmunoprecipitation

Coimmunoprecipitation was performed using a Pierce Coimmunoprecipitation Kit (Invitrogen) as instructed in the manual. The HUVECs were infected with ad-*PFKFB3* or control vehicle for 48 h and then lysed in lysis buffer added with 1X protease/phosphatase inhibitor cocktail and 1 mM PMSF. The anti-PFKFB3 antibody (Proteintech, Rosemont, USA) was immobilized with AminoLink Plus coupling resin for 2 h at room temperature. The cell lysates were incubated with anti-PFKFB3-conjugated agarose resin at 4 °C overnight. After elution, the coimmunoprecipitation samples were analyzed by Western blot.

4.12. Quantitative real-time PCR

RNA was extracted using TRIzol (Invitrogen), after which DNase treatment (Takara, Kyoto, Japan) was performed. Reverse transcription was carried out with a cDNA Synthesis Kit (Takara). Quantitative Real-Time PCR (qPCR) was performed using TB Green Premix Ex Taq™ (Takara) by ViiA 7 (Applied Biosystems, DE, USA). Relative mRNA levels were quantified by normalizing with β-actin detected using commercially available predesigned primers (Sangon Biotech). The primer sequences of *PFKFB3* are as follows: forward, 5′-GATGCCCTTCAGGAAAGCCT -3′; reverse, 5′- TCCCCGACGTTGAACACTTT -3′.

4.13. DNA repair reporter assay

DNA repair reporter (DRR) assay for the activity of homologous recombination repair (HR) and non-homologous end joining (NHEJ) was performed as previously described [71,72]. The HUVECs seeded on six-well plates were transfected with 1.6 μg pLCN-DSB Repair Reporter, 1.6 μg pCAGGS DSB Repair Reporter mCherry Donor EF1 BFP plasmid, and 1.6 μg pCBAsceI plasmid with Lipofectamine 2000. pCBAsceI plasmid alone was used as a negative control. GFP and mCherry signal analysis was conducted using flow cytometry on a FACS scan flow cytometry machine (Beckman, CA, USA) 48 h after transfection. The following plasmids were used: pLCN-DSB Repair Reporter (Addgene, Cat. No. 98895), pCAGGS DSB Repair Reporter mCherry Donor EF1a BFP (Addgene, Cat. No. 98896), and pCBASceI (Addgene, Cat. No. 26477).

4.14. Alkaline comet assay

DNA damage levels were evaluated using the alkaline comet assay (Trevigen, MD, USA). The HUVECs seeded on six-well plates were treated with 300 μM H_2O_2 for 30 min, washed in PBS, and left to recover in fresh media for 2 h. The comet assay was conducted according to the manufacturer's instructions. Briefly, the HUVEC suspension (1×10^5 cells/mL) in ice-cold PBS was harvested after digesting with trypsin and washed once in PBS. Up to 50 μl of this cell suspension was used for mixing with 450 μL pre-warmed low-melting-point agarose. Then, 50 μl of these mixtures were placed on each well of comet slides. After gel solidification, the slides were immersed in a lysis solution at 4 °C overnight. Afterward, the slides were incubated in an alkaline solution (1 mM EDTA, 200 mM NaOH, pH > 13) for 40 min in the dark for DNA unwinding. The slides were then placed in a horizontal electrophoresis chamber filled with an alkaline solution for electrophoresis (21 V, 30 min). For gel dehydration, the slides were placed in 70% ethanol for 5 min. After air drying, all samples were stained with SYBR Gold (Invitrogen). Five fields of view per slide were taken using a confocal microscope (× 100 magnification). The tail moment was calculated using specialized CometAssay Analysis Software (Trevigen).

4.15. SA-β-Gal staining

For senescence induction, the HUVECs were incubated in 700 μM H_2O_2 at 37 °C for 30 min H_2O_2 treatment was terminated by a gentle washing process with PBS. The cells were then infected with Ads and cultured for 48 h with different treatments that will be described later in individual figure legends. Intracellular senescence-associated-β-galactosidase (SA-β-Gal) activity was assayed using an SA-β-Gal Staining Kit (Beyotime) according to the manufacturer's instructions. Senescent cells were identified as bluish-green-stained cells under a phase-contrast microscope. The percentage of SA-β-Gal-positive cells was determined by the mean of five random fields (× 100 magnification).

4.16. Intracellular ROS measurement

The intracellular ROS levels were determined using a ROS Assay Kit (Beyotime) following the protocols. Briefly, the HUVECs were treated under different conditions and incubated with 2′,7′-Dichlorodihydrofluorescein diacetate (DCFH-DA, with excitation and emission spectrum peak wavelengths of 488 nm/525 nm) for 30 min at 37 °C. Then, the cells were harvested and analyzed on a FACS scan flow cytometry machine (Beckman).

4.17. Cell bioenergy tests

ATP production rate, extracellular acidification rate (ECAR), and oxygen consumption rate (OCR) were measured with a Real-Time ATP Rate Kit, Mito Stress Test Kit, and Glycolysis Rate Kit, respectively, using a Seahorse XFe24 Analyzer (Agilent Technologies, CA, USA). The HUVECs were seeded on XFe24-well microplates (20,000 cells/well), and the Seahorse 1640 media were supplemented with 2 mM L-glutamine, 10 mM glucose, and 1 mM sodium pyruvate. The sensor cartridge was incubated with 1 mL XF Calibrant (pH 7.4) per well at 37 °C without CO_2 overnight. OCR and ECAR were detected by sequential injections of compounds at the specified time points according to the instructions of the manufacturer. Data were normalized by cell numbers measured by the YOPRO®-1 Assay (Thermo Fisher Scientific) and analyzed using Wave software (Agilent Technologies).

4.18. Intracellular metabolite measurement

ATP measurements were performed using an ATP Determination Kit (Invitrogen). The HUVECs were lysed on ice using a lysis buffer containing 20 mM Tris, 100 mM NaCl, 1 mM EDTA, and 0.5% Triton X-100 supplemented with 1 × protease/phosphatase inhibitor cocktail and 1 mM PMSF. Reagents were added according to the instructions of the manufacturer, and the luminescence was determined using a luminometer.

For colorimetric measurements of lactic acid and pyruvate, the HUVECs were lysed by ultrasonic decomposition on ice. Reagents were added following the manufacturer's instructions for the Lactic Acid Assay Kit and Pyruvate Assay Kit (Nanjing Jiancheng Bioengineer Institute, Nanjing, China). Then, 530 nm absorbance for lactic acid production and 505 nm absorbance for pyruvate production were measured at 25 °C.

The NAD pool was detected using an NAD+/NADH Quantification Kit through the colorimetric method (Abcam, Cambridge, UK) according to the manufacturer's instructions. Colorimetric measurements were

made at 450 nm absorbance at 25 °C. The NAD pool concentrations were determined from a standard calibration curve. The value was normalized by protein concentrations.

4.19. Statistical analysis

All data originated from at least three independent experiments and were presented as mean ± standard deviation (SD). Differences among experimental groups were analyzed by two-tailed Student's t-test or one-way ANOVA (followed by Turkey's or Sidak's test) using GraphPad Prism 9.0. Significance was set at $P < 0.05$.

4.20. Study approval

Animals were treated in accordance with the ARRIVE guidelines and the National Research Council's Guide for the Care and Use of Laboratory Animals and approved by the Ethics committee of Shanghai General Hospital, Shanghai Jiao Tong University School of Medicine, Shanghai, China (reference number: 2019-A049-01).

Human samples were collected with informed consent following the guidelines of the Helsinki Declaration. This study was approved by the Ethics committee of Shanghai General Hospital, Shanghai Jiao Tong University School of Medicine, Shanghai, China (reference number: 2020SQ100).

Author contributions

DS, FW and XX designed this study. DS and SC executed the experiments. DS, SL and NW collected the human specimens, carried out experimental work and analyzed data. DS, LX and SZ maintained the mice and analyzed data. FW, XX, QG, SZ and HL provided resources, supervised the experiments, and participated in the data analyses. DS and FW wrote the article with input from all authors. All authors proofread the manuscript.

Declaration of competing interest

The authors declare that they have no known competing financial interests or personal relationships that could have appeared to influence the work reported in this paper.

Data availability

Data will be made available on request.

Acknowledgements

We especially thank Dr. Xinming Qi from the Shanghai Institute of Materia Medica, Chinese Academy of Sciences for his technical support. This work was supported by the National Natural Science Foundation of China [grant numbers 81970846, 81970812]; Science and Technology Research Project of Songjiang District [grant number 2020SJ300]; National Key R&D Program of China [grant numbers 2016YFC0904800, 2019YFC0840607]; and National Science and Technology Major Project of China [grant number 2017ZX09304010].

Appendix A. Supplementary data

Supplementary data to this article can be found online at https://doi.org/10.1016/j.redox.2022.102589.

References

[1] J.L. Harding, M.E. Pavkov, D.J. Magliano, J.E. Shaw, E.W. Gregg, Global trends in diabetes complications: a review of current evidence, Diabetologia 62 (1) (2019) 3–16.

[2] P. Saeedi, I. Petersohn, P. Salpea, B. Malanda, S. Karuranga, N. Unwin, et al., Global and regional diabetes prevalence estimates for 2019 and projections for 2030 and 2045: results from the international diabetes federation diabetes atlas, in: 9(th) editionDiabetes Research and Clinical Practice, vol. 157, 2019, 107843.

[3] H.P. Hammes, Diabetic retinopathy: hyperglycaemia, oxidative stress and beyond, Diabetologia 61 (1) (2018) 29–38.

[4] M. Brownlee, The pathobiology of diabetic complications: a unifying mechanism, Diabetes 54 (6) (2005) 1615–1625.

[5] X. Du, T. Matsumura, D. Edelstein, L. Rossetti, Z. Zsengellér, C. Szabó, et al., Inhibition of GAPDH activity by poly(ADP-ribose) polymerase activates three major pathways of hyperglycemic damage in endothelial cells, J. Clin. Invest. 112 (7) (2003) 1049–1057.

[6] M. Lorenzi, D.F. Montisano, S. Toledo, A. Barrieux, High glucose induces DNA damage in cultured human endothelial cells, J. Clin. Invest. 77 (1) (1986) 322–325.

[7] L. Quagliaro, L. Piconi, R. Assaloni, L. Martinelli, E. Motz, A. Ceriello, Intermittent high glucose enhances apoptosis related to oxidative stress in human umbilical vein endothelial cells: the role of protein kinase C and NAD(P)H-oxidase activation, Diabetes 52 (11) (2003) 2795–2804.

[8] Y.T. He, S.S. Xing, L. Gao, J. Wang, Q.C. Xing, W. Zhang, Ginkgo biloba attenuates oxidative DNA damage of human umbilical vein endothelial cells induced by intermittent high glucose, Pharmazie 69 (3) (2014) 203–207.

[9] L. Zeng, Q.F. Ding, T.Y. Xu, F. Luo, N. Ge, S.T. Li, [The role of DNA double-strain damage repairing mechanisms in diabetic atheroscolersis], J. Sichuan Univ. Med. Sci. 48 (2) (2017) 191–196.

[10] V. Kumar, R. Agrawal, A. Pandey, S. Kopf, M. Hoeffgen, S. Kaymak, et al., Compromised DNA repair is responsible for diabetes-associated fibrosis, EMBO J. 39 (11) (2020), e103477.

[11] J. Pang, C. Xi, Y. Dai, H. Gong, T.M. Zhang, Altered expression of base excision repair genes in response to high glucose-induced oxidative stress in HepG2 hepatocytes, Med. Sci. Mon. Int. Med. J. Exp. Clin. Res. : Int. Med. J. Exper. Clin. Res. 18 (7) (2012) Br281–B285.

[12] H. Mizukami, K. Takahashi, W. Inaba, K. Tsuboi, S. Osonoi, T. Yoshida, et al., Involvement of oxidative stress-induced DNA damage, endoplasmic reticulum stress, and autophagy deficits in the decline of beta-cell mass in Japanese type 2 diabetic patients, Diabetes Care 37 (7) (2014) 1966–1974.

[13] S. Tornovsky-Babeay, D. Dadon, O. Ziv, E. Tzipilevich, T. Kadosh, R. Schyr-Ben Haroush, et al., Type 2 diabetes and congenital hyperinsulinism cause DNA double-strand breaks and p53 activity in beta cells, Cell Metabol. 19 (1) (2014) 109–121.

[14] S. Bhatt, M.K. Gupta, M. Khamaisi, R. Martinez, M.A. Gritsenko, B.K. Wagner, et al., Preserved DNA damage checkpoint pathway protects against complications in long-standing type 1 diabetes, Cell Metabol. 22 (2) (2015) 239–252.

[15] S. Li, J. Deng, D. Sun, S. Chen, X. Yao, N. Wang, et al., FBXW7 alleviates hyperglycemia-induced endothelial oxidative stress injury via ROS and PARP inhibition, Redox Biol. 58 (2022), 102530.

[16] T. Kitamura, The role of FOXO1 in beta-cell failure and type 2 diabetes mellitus, Nat. Rev. Endocrinol. 9 (10) (2013) 615–623.

[17] B. Ponugoti, G. Dong, D.T. Graves, Role of forkhead transcription factors in diabetes-induced oxidative stress, Exp. Diabetes Res. 2012 (2012), 939751.

[18] D. Jian, Y. Wang, L. Jian, H. Tang, L. Rao, K. Chen, et al., METTL14 aggravates endothelial inflammation and atherosclerosis by increasing FOXO1 N6-methyladeosine modifications, Theranostics 10 (20) (2020) 8939–8956.

[19] P.K. Battiprolu, B. Hojayev, N. Jiang, Z.V. Wang, X. Luo, M. Iglewski, et al., Metabolic stress-induced activation of FoxO1 triggers diabetic cardiomyopathy in mice, J. Clin. Invest. 122 (3) (2012) 1109–1118.

[20] K. Gopal, R. Al Batran, T.R. Altamimi, A.A. Greenwell, C.T. Saed, S.A. Tabatabaei Dakhili, et al., FoxO1 inhibition alleviates type 2 diabetes-related diastolic dysfunction by increasing myocardial pyruvate dehydrogenase activity, Cell Rep. 35 (1) (2021), 108935.

[21] K. Zhang, L. Li, Y. Qi, X. Zhu, B. Gan, R.A. DePinho, et al., Hepatic suppression of Foxo1 and Foxo3 causes hypoglycemia and hyperlipidemia in mice, Endocrinology 153 (2) (2012) 631–646.

[22] W. Zhang, S. Patil, B. Chauhan, S. Guo, D.R. Powell, J. Le, et al., FoxO1 regulates multiple metabolic pathways in the liver: effects on gluconeogenic, glycolytic, and lipogenic gene expression, J. Biol. Chem. 281 (15) (2006) 10105–10117.

[23] X. Xiong, R. Tao, R.A. DePinho, X.C. Dong, Deletion of hepatic FoxO1/3/4 genes in mice significantly impacts on glucose metabolism through downregulation of gluconeogenesis and upregulation of glycolysis, PLoS One 8 (8) (2013), e74340.

[24] K. Wilhelm, K. Happel, G. Eelen, S. Schoors, M.F. Oellerich, R. Lim, et al., FOXO1 couples metabolic activity and growth state in the vascular endothelium, Nature 529 (7585) (2016) 216–220.

[25] Y. Behl, P. Krothapalli, T. Desta, S. Roy, D.T. Graves, FOXO1 plays an important role in enhanced microvascular cell apoptosis and microvascular cell loss in type 1 and type 2 diabetic rats, Diabetes 58 (4) (2009) 917–925.

[26] C. Jang, Z. Arany, Metabolism: sweet enticements to move, Nature 500 (7463) (2013) 409–411.

[27] E.E. Bankoglu, C. Schuele, H. Stopper, Cell survival after DNA damage in the comet assay, Arch. Toxicol. 95 (12) (2021) 3803–3813.

[28] R. Di Micco, V. Krizhanovsky, D. Baker, F. d'Adda di Fagagna, Cellular senescence in ageing: from mechanisms to therapeutic opportunities, Nat. Rev. Mol. Cell Biol. 22 (2) (2021) 75–95.

[29] A.N. Blackford, S.P. Jackson, ATM, ATR, and DNA-PK: the trinity at the heart of the DNA damage response, Molecular cell 66 (6) (2017) 801–817.

[30] R. Scully, A. Panday, R. Elango, N.A. Willis, DNA double-strand break repair-pathway choice in somatic mammalian cells, Nat. Rev. Mol. Cell Biol. 20 (11) (2019) 698–714.

[31] K. De Bock, M. Georgiadou, S. Schoors, A. Kuchnio, B.W. Wong, A.R. Cantelmo, et al., Role of PFKFB3-driven glycolysis in vessel sprouting, Cell 154 (3) (2013) 651–663.
[32] J. Sabbatinelli, F. Prattichizzo, F. Olivieri, A.D. Procopio, M.R. Rippo, A. Giuliani, Where metabolism meets senescence: focus on endothelial cells, Front. Physiol. 10 (2019) 1523.
[33] L. Rajman, K. Chwalek, D.A. Sinclair, Therapeutic potential of NAD-boosting molecules: the in vivo evidence, Cell Metabol. 27 (3) (2018) 529–547.
[34] X. Tang, Y.X. Luo, H.Z. Chen, D.P. Liu, Mitochondria, endothelial cell function, and vascular diseases, Front. Physiol. 5 (2014) 175.
[35] J.F. Passos, G. Nelson, C. Wang, T. Richter, C. Simillion, C.J. Proctor, et al., Feedback between p21 and reactive oxygen production is necessary for cell senescence, Mol. Syst. Biol. 6 (2010) 347.
[36] T. Oliveira, T. Goldhardt, M. Edelmann, T. Rogge, K. Rauch, N.D. Kyuchukov, et al., Effects of the novel PFKFB3 inhibitor KAN0438757 on colorectal cancer cells and its systemic toxicity evaluation in vivo, Cancers 13 (5) (2021).
[37] M. Kanwar, R.A. Kowluru, Role of glyceraldehyde 3-phosphate dehydrogenase in the development and progression of diabetic retinopathy, Diabetes 58 (1) (2009) 227–234.
[38] M.G. Clark, E.J. Barrett, M.G. Wallis, M.A. Vincent, S. Rattigan, The microvasculature in insulin resistance and type 2 diabetes, Semin. Vasc. Med. 2 (1) (2002) 21–31.
[39] W. Patton, H. Gillespie, L. Frew, M. Burns, S. Lewis, U. Chakravarthy, The effects of high ambient glucose on the radiosensitivity of retinal microvascular endothelial cells and pericytes, Curr. Eye Res. 24 (1) (2002) 51–57.
[40] M. Viebahn, M.E. Barricks, M.D. Osterloh, Synergism between diabetic and radiation retinopathy: case report and review, Br. J. Ophthalmol. 75 (10) (1991) 629–632.
[41] A.N. Bhatt, A. Chauhan, S. Khanna, Y. Rai, S. Singh, R. Soni, et al., Transient elevation of glycolysis confers radio-resistance by facilitating DNA repair in cells, BMC Cancer 15 (2015) 335.
[42] E.V. Efimova, S. Takahashi, N.A. Shamsi, D. Wu, E. Labay, O.A. Ulanovskaya, et al., Linking cancer metabolism to DNA repair and accelerated senescence, Mol. Cancer Res. 14 (2) (2016) 173–184.
[43] E. Giovannucci, D.M. Harlan, M.C. Archer, R.M. Bergenstal, S.M. Gapstur, L. A. Habel, et al., Diabetes and cancer: a consensus report, Diabetes Care 33 (7) (2010) 1674–1685.
[44] S.C. Lee, J.C. Chan, Evidence for DNA damage as a biological link between diabetes and cancer, Chin. Med. J. 128 (11) (2015) 1543–1548.
[45] S. Yang, J. Chintapalli, L. Sodagum, S. Baskin, A. Malhotra, K. Reiss, et al., Activated IGF-1R inhibits hyperglycemia-induced DNA damage and promotes DNA repair by homologous recombination, Am. J. Physiol. Ren. Physiol. 289 (5) (2005) F1144–F1152.
[46] K. Wang, T. Zhang, Q. Dong, E.C. Nice, C. Huang, Y. Wei, Redox homeostasis: the linchpin in stem cell self-renewal and differentiation, Cell Death Dis. 4 (2013) e537.
[47] L.O. Klotz, C. Sánchez-Ramos, I. Prieto-Arroyo, P. Urbánek, H. Steinbrenner, M. Monsalve, Redox regulation of FoxO transcription factors, Redox Biol. 6 (2015) 51–72.
[48] M. Tajes Orduna, C. Pelegri Gabalda, J. Vilaplana Hortensi, M. Pallas Lliberia, A. Camins Espuny, An evaluation of the neuroprotective effects of melatonin in an in vitro experimental model of age-induced neuronal apoptosis, J. Pineal Res. 46 (3) (2009) 262–267.
[49] H. Huang, K.M. Regan, Z. Lou, J. Chen, D.J. Tindall, CDK2-dependent phosphorylation of FOXO1 as an apoptotic response to DNA damage, Science (New York, NY) 314 (5797) (2006) 294–297.
[50] H. Huang, D.J. Tindall, CDK2 and FOXO1: a fork in the road for cell fate decisions, Cell Cycle 6 (8) (2007) 902–906.
[51] B. Halder, S. Das Gupta, A. Gomes, Black Tea Polyphenols Induce Human Leukemic Cell Cycle Arrest by Inhibiting Akt Signaling, vol. 279, 2012, pp. 2876–2891, 16.
[52] Y. Zhu, X. Geng, C. Stone, S. Guo, S. Syed, Y. Ding, Forkhead Box 1(FoxO1) mediates psychological stress-induced neuroinflammation, Neurol. Res. (2022) 1–13.
[53] F. Rodier, J.P. Coppé, C.K. Patil, W.A. Hoeijmakers, D.P. Muñoz, S.R. Raza, et al., Persistent DNA damage signalling triggers senescence-associated inflammatory cytokine secretion, Nat. Cell Biol. 11 (8) (2009) 973–979.
[54] I. Van Hove, L. De Groef, B. Boeckx, E. Modave, T.T. Hu, K. Beets, et al., Single-cell transcriptome analysis of the Akimba mouse retina reveals cell-type-specific insights into the pathobiology of diabetic retinopathy, Diabetologia 63 (10) (2020) 2235–2248.
[55] M.S. Ola, D.A. Berkich, Y. Xu, M.T. King, T.W. Gardner, I. Simpson, et al., Analysis of glucose metabolism in diabetic rat retinas, Am. J. Physiol. Endocrinol. Metabol. 290 (6) (2006) E1057–E1067.
[56] E. Shosha, L. Qin, T. Lemtalsi, S.A.H. Zaidi, M. Rojas, Z. Xu, et al., Investigation of retinal metabolic function in type 1 diabetic akita mice, Front Cardiovasc Med 9 (2022), 900640.
[57] M. Rudnicki, G. Abdifarkosh, E. Nwadozi, S.V. Ramos, A. Makki, D.M. Sepa-Kishi, et al., Endothelial-specific FoxO1 depletion prevents obesity-related disorders by increasing vascular metabolism and growth, Elife 7 (2018).
[58] K.R. Cargill, C.A. Stewart, E.M. Park, K. Ramkumar, C.M. Gay, R.J. Cardnell, et al., Targeting MYC-enhanced glycolysis for the treatment of small cell lung cancer, Cancer Metabol. 9 (1) (2021) 33.
[59] F.-L. Li, J.-P. Liu, R.-X. Bao, G. Yan, X. Feng, Y.-P. Xu, et al., Acetylation accumulates PFKFB3 in cytoplasm to promote glycolysis and protects cells from cisplatin-induced apoptosis, Nat. Commun. 9 (1) (2018) 508.
[60] N.M.S. Gustafsson, K. Farnegardh, N. Bonagas, A.H. Ninou, P. Groth, E. Wiita, et al., Targeting PFKFB3 radiosensitizes cancer cells and suppresses homologous recombination, Nat. Commun. 9 (1) (2018) 3872.
[61] C.M. Galindo, F.A. Oliveira Ganzella, G. Klassen, E.A. Souza Ramos, A. Acco, Nuances of PFKFB3 signaling in breast cancer, Clin. Breast Cancer 22 (4) (2022) e604–e614.
[62] S.M. Kuosmanen, V. Sihvola, E. Kansanen, M.U. Kaikkonen, A.L. Levonen, MicroRNAs mediate the senescence-associated decline of NRF2 in endothelial cells, Redox Biol. 18 (2018) 77–83.
[63] Y. Yang, M. Zhao, X.J. Yu, L.Z. Liu, X. He, J. Deng, et al., Pyridostigmine regulates glucose metabolism and mitochondrial homeostasis to reduce myocardial vulnerability to injury in diabetic mice, Am. J. Physiol. Endocrinol. Metabol. 317 (2) (2019). E312-e26.
[64] M. Qian, Z. Liu, L. Peng, X. Tang, F. Meng, Y. Ao, et al., Boosting ATM activity alleviates aging and extends lifespan in a mouse model of progeria, Elife 7 (2018).
[65] F. Bartoli-Leonard, F.L. Wilkinson, A. Schiro, F. Serracino Inglott, M.Y. Alexander, R. Weston, Loss of SIRT1 in diabetes accelerates DNA damage-induced vascular calcification, Cardiovasc. Res. 117 (3) (2021) 836–849.
[66] M.J. Charron, S. Bonner-Weir, Implicating PARP and NAD+ depletion in type I diabetes, Nat. Med. 5 (3) (1999) 269–270.
[67] J. Li, M.S. Bonkowski, S. Moniot, D. Zhang, B.P. Hubbard, A.J. Ling, et al., A conserved NAD(+) binding pocket that regulates protein-protein interactions during aging, Science (New York, NY) 355 (6331) (2017) 1312–1317.
[68] B. Clem, S. Telang, A. Clem, A. Yalcin, J. Meier, A. Simmons, et al., Small-molecule inhibition of 6-phosphofructo-2-kinase activity suppresses glycolytic flux and tumor growth, Mol. Cancer Therapeut. 7 (1) (2008) 110–120.
[69] S. Crespo-Garcia, P.R. Tsuruda, A. Dejda, R.D. Ryan, F. Fournier, S.Y. Chaney, et al., Pathological angiogenesis in retinopathy engages cellular senescence and is amenable to therapeutic elimination via BCL-xL inhibition, Cell Metabol. 33 (4) (2021) 818–832, e7.
[70] A. Sawasdichai, H.-T. Chen, N. Abdul Hamid, P.-S. Jayaraman, K. Gaston, In situ subcellular fractionation of adherent and non-adherent mammalian cells, JoVE 41 (2010) 1958.
[71] N. Arnoult, A. Correia, J. Ma, A. Merlo, S. Garcia-Gomez, M. Maric, et al., Regulation of DNA repair pathway choice in S and G2 phases by the NHEJ inhibitor CYREN, Nature 549 (7673) (2017) 548–552.
[72] T. Fukumoto, H. Zhu, T. Nacarelli, S. Karakashev, N. Fatkhutdinov, S. Wu, et al., N (6)-Methylation of adenosine of FZD10 mRNA contributes to PARP inhibitor resistance, Cancer Res. 79 (11) (2019) 2812–2820.